Structural Safety 112 (2025) 102539

Contents lists available at ScienceDirect

Structural Safety

journal homepage: www.elsevier.com/locate/strusafe

Yet another Bayesian active learning reliability analysis method

Chao Dang [a,*], Tong Zhou [b], Marcos A. Valdebenito [a], Matthias G.R. Faes [a]

[a] Chair for Reliability Engineering, TU Dortmund University, Leonhard-Euler-Straße 5, 44227 Dortmund, Germany
[b] Department of Civil and Environmental Engineering, The Hong Kong Polytechnic University, Hong Kong, China

ARTICLE INFO

Keywords:
Structural reliability analysis
Extremely small failure probability
Bayesian active learning
Stopping criterion
Learning function

ABSTRACT

The well-established Bayesian failure probability inference (BFPI) framework offers a solid foundation for developing new Bayesian active learning reliability analysis methods. However, there remains an open question regarding how to effectively leverage the posterior statistics of the failure probability to design the two key components for Bayesian active learning: the stopping criterion and learning function. In this study, we present another innovative Bayesian active learning reliability analysis method, called 'Weakly Bayesian Active Learning Quadrature' (WBALQ), which builds upon the BFPI framework to evaluate extremely small failure probabilities. Instead of relying on the posterior variance, we propose a more computationally feasible measure of the epistemic uncertainty in the failure probability by examining its posterior first absolute central moment. Based on this measure and the posterior mean of the failure probability, a new stopping criterion is devised. A recently developed numerical integrator is then employed to approximate the two analytically intractable terms inherent in the stopping criterion. Furthermore, a new learning function is proposed, which is partly derived from the epistemic uncertainty measure. The performance of the proposed method is demonstrated by five numerical examples. It is found that our method is able to assess extremely small failure probabilities with satisfactory accuracy and efficiency.

1. Introduction

Structural reliability analysis is a critical tool for evaluating the ability of an engineered structure to perform its intended functions – such as safety, serviceability and durability – while accounting for various uncertainties inherent in both internal structural properties and external environmental conditions. In a purely probabilistic setting, structural reliability analysis usually involves calculating the complement of reliability, the so-called failure probability P_f, which is mathematically defined by an often intractable multiple integral:

$$P_f = \int_{\mathcal{X}} I(\boldsymbol{x}) f_{\boldsymbol{X}}(\boldsymbol{x}) \mathrm{d}\boldsymbol{x}, \tag{1}$$

in which $\boldsymbol{X} = [X_1, X_2, \ldots, X_d] \in \mathcal{X} \subseteq \mathbb{R}^d$ is a vector of d basic continuous random variables with support $\mathcal{X}$; $\boldsymbol{x}$ denotes a realization of $\boldsymbol{X}$; $f_{\boldsymbol{X}} : \mathbb{R}^d \to \mathbb{R}_{\geq 0}$ is the joint probability density function (PDF) of $\boldsymbol{X}$; $I : \mathbb{R}^d \to \{0, 1\}$ is the indicator function: $I = 1$ if $g(\boldsymbol{x}) < 0$, and $I = 0$ otherwise; $g : \mathbb{R}^d \to \mathbb{R}$ represents the performance function (also known as the limit state function), and a failure occurs when g takes a negative value.

Numerical methods for structural reliability analysis have been developed since Freudenthal published his first work on safety of structures [1,2]. These methods include Monte Carlo simulation (MCS) and its variants (e.g., importance sampling (IS) [3–6], subset simulation [7–9], directional simulation [10,11] and line sampling [12–14]), first-/second- order reliability method [15,16], statistical moments based methods [17–19] and surrogate-assisted methods (e.g., response surface method [20], polynomial chaos expansion [21], support vector regression [22], Kriging [23]), among many others. One can refer to [24] for an excellent review of existing structural reliability analysis methods. Over the past decade, a particular class of adaptive methods, known as active learning reliability analysis methods, has received a great deal of attention. This is largely because they have demonstrated the ability to provide accurate failure probability estimates with a relatively small number of performance function evaluations. Two milestone contributions in this area are the efficient global reliability analysis [25] and the Active Kriging Monte Carlo simulation (AK-MCS) [26]. The latter is regarded as the cornerstone of various methods devised by modifying one or more aspects of AK-MCS. For a comprehensive review of recent advances in active learning reliability analysis methods, the reader is referred to [27,28].

The first author and his collaborators have recently advanced the development of a specialized type of active learning for structural reliability analysis, namely Bayesian active learning. The resulting

* Corresponding author.
E-mail address: chao.dang@tu-dortmund.de (C. Dang).

https://doi.org/10.1016/j.strusafe.2024.102539
Received 30 May 2024; Received in revised form 15 September 2024; Accepted 16 September 2024
Available online 20 September 2024

methods, referred to as Bayesian active learning reliability analysis methods, feature a unique fusion of Bayesian inference and active learning. The basic idea can be roughly summarized as follows: (1) estimation of the failure probability integral (Eq. (1)) is first interpreted as a Bayesian inference problem; (2) active learning of the failure probability value is then set up based on the posterior statistics of the failure probability. The first idea is exposed in [29], where the posterior mean and an upper bound on the posterior variance of the failure probability are derived given a Gaussian process (GP) prior is placed over the performance function. On this basis, a Bayesian active learning method called 'Active Learning Probabilistic Integration' (ALPI) is also developed. The ALPI method is further improved by the 'Parallel Adaptive Bayesian Quadrature' (PABQ) [30] method to estimate (extremely) small failure probabilities and to allow parallel distributed processing. It is important to note that the upper bound of the posterior variance of the failure probability tends to overestimate the true variance in most instances. Thus, the Bayesian approach to failure probability estimation is revisited in [31]. The authors offer a principled Bayesian failure probability inference (BFPI) framework, where an expression for the posterior variance of the probability of failure is obtained. From the perspective of the second-order posterior statistics, the BFPI framework provides a relatively comprehensive Bayesian treatment of the failure probability integral, which can therefore serve as a good starting point for developing Bayesian active learning reliability analysis methods. Unfortunately, the posterior variance of the failure probability is analytically intractable and computationally demanding, making it difficult to use in a Bayesian active learning context.

To develop Bayesian active learning methods based on the BFPI framework for structural reliability analysis, two types of ideas have been explored. The first one involves designing the two key components for Bayesian active learning (i.e., stopping criterion and learning function) using only the posterior mean of the failure probability. Examples in this category include the 'Partially Bayesian Active Learning Cubature' (PBALC) method [32] and the 'Semi-Bayesian Active Learning Quadrature' (SBALQ) method [33]. The latter utilizes not only the posterior mean but also the posterior variance of the failure probability, albeit with some simplification. ALPI [29] and PABQ [29] fall into this category, though they were developed before the BPFI framework. In addition, there are the 'Parallel Bayesian Probabilistic Integration' (PBPI) method [34] and 'Quasi-Bayesian Active Learning Cubature' (QBALC) method [35]. Despite significant progress, developing an effective structural reliability analysis method based on the BFPI framework remains an open problem. In particular, it is still challenging to create a method that can produce a failure probability estimate with a prescribed level of accuracy, while minimizing the number of performance function evaluations.

To fill the research gap, this work presents another novel Bayesian active learning reliability analysis method, called 'Weakly Bayesian Active Learning Quadrature' (WBALQ), by leveraging the BFPI framework. The method is expected to be able to evaluate extremely small failure probabilities, which is one of the key challenges in structural reliability analysis. The main contributions can be summarized as follows:

- An upper bound on the first absolute central moment of the posterior failure probability is derived, providing a more computationally feasible alternative to the posterior variance as a measure of epistemic uncertainty in the failure probability;
- A new stopping criterion, a key component of Bayesian active learning, is proposed based on the epistemic uncertainty measure and posterior mean of the failure probability. It ensures that the failure probability estimate reaches a certain level of accuracy before terminating the iterative process;
- Additionally, a new learning function, another essential element for Bayesian active learning, is developed, which is partially derived from the epistemic uncertainty measure. This function guides the section of the most informative points for evaluating the performance function;
- The performance of the proposed WBALQ method is evaluated against several representative existing Bayesian active learning reliability analysis methods using five benchmark numerical examples.

The rest of this paper is structured as follows. Section 2 provides a general overview of several related studies. The proposed WBALQ method is introduced in Section 3. Five benchmark numerical examples are studied in Section 4 to demonstrate the performance of the proposed method against several existing methods. The paper closes with some concluding remarks in Section 5.

2. Review of relevant literature

This section provides a brief introduction to the BFPI framework [31] that underpins our new development. In addition, it also summarizes some typical existing Bayesian active learning methods for structural reliability analysis. To be consistent with the setting of the proposed method, the BFPI framework is restated in standard normal space rather than the physical space. Let us first introduce a transformation T (e.g., Nataf transformation or Rosenblatt transformation) that can transform the original random vector $\boldsymbol{X}$ into a standard normal one $\boldsymbol{U} = [U_1, U_2, \dots, U_d] \in \mathcal{U} \subseteq \mathbb{R}^d$, i.e., $\boldsymbol{U} = T(\boldsymbol{X})$. Then, the original performance function g can be rewritten as $\mathcal{G}(\boldsymbol{u}) = g(T^{-1}(\boldsymbol{u}))$, where $\mathcal{G} = g \circ T^{-1}$ is called the transformed performance function. The corresponding indicator function and failure probability are denoted as $\mathcal{I}$ and $\mathcal{P}_f$ respectively.

2.1. Bayesian failure probability inference

2.1.1. Prior distribution

We model our prior beliefs about $\mathcal{G}$ using a GP, i.e.,

$$\tilde{\mathcal{G}}_0(\boldsymbol{u}) \sim \mathcal{GP}(m_{\tilde{\mathcal{G}}_0}(\boldsymbol{u}), k_{\tilde{\mathcal{G}}_0}(\boldsymbol{u}, \boldsymbol{u}')), \tag{2}$$

where $\tilde{\mathcal{G}}_0$ represents the prior distribution of $\mathcal{G}$; $m_{\tilde{\mathcal{G}}_0}(\boldsymbol{u})$ and $k_{\tilde{\mathcal{G}}_0}(\boldsymbol{u}, \boldsymbol{u}')$ denote the prior mean and covariance functions, respectively. Among the various options available, we adopt the commonly-used constant and squared exponential kernel for the prior mean and covariance functions, respectively:

$$m_{\tilde{\mathcal{G}}_0}(\boldsymbol{u}) = b, \tag{3}$$

$$k_{\tilde{\mathcal{G}}_0}(\boldsymbol{u}, \boldsymbol{u}') = \sigma_0^2 \exp\left(-\frac{1}{2}(\boldsymbol{u} - \boldsymbol{u}')\boldsymbol{\Sigma}^{-1}(\boldsymbol{u} - \boldsymbol{u}')^\top\right), \tag{4}$$

where $b \in \mathbb{R}$; $\sigma_0 > 0$ denotes the prior standard deviation; $\boldsymbol{\Sigma} = \mathrm{diag}\left\{l_1^2, l_2^2, \dots, l_d^2\right\}$ with $l_i > 0$ being the lengthscale in ith dimension. With the above settings, the GP prior is parameterized by the $d + 2$ hyper-parameters collected in $\boldsymbol{\vartheta} = \left\{b, \sigma_0, l_1, l_2, \dots, l_d\right\}$. Note that the choice of prior mean and covariance functions does not affect the generality of the BFPI framework.

2.1.2. Estimating the hyper-parameters

Let $\boldsymbol{\mathcal{D}} = \{\boldsymbol{\mathcal{U}}, \boldsymbol{\mathcal{Y}}\}$ be a dataset consisting of n input–output pairs of the function $\mathcal{G}$, where $\boldsymbol{\mathcal{U}}$ is an n-by-d matrix whose ith row is the ith input point $\boldsymbol{u}^{(i)}$ and $\boldsymbol{\mathcal{Y}}$ is an n-by-1 column vector whose ith component is the ith $\mathcal{G}$-function observation $y^{(i)}$ ($y^{(i)} = \mathcal{G}(\boldsymbol{u}^{(i)})$). The hyper-parameters $\boldsymbol{\vartheta}$ can be fitted to the dataset $\boldsymbol{\mathcal{D}}$ by maximizing the log likelihood:

$$\log p(\boldsymbol{\mathcal{Y}}|\boldsymbol{\mathcal{U}}, \boldsymbol{\vartheta}) = -\frac{1}{2}\left[(\boldsymbol{\mathcal{Y}} - b)^\top \boldsymbol{K}_{\tilde{\mathcal{G}}_0}^{-1}(\boldsymbol{\mathcal{Y}} - b) + \log|\boldsymbol{K}_{\tilde{\mathcal{G}}_0}| + n\log 2\pi\right], \tag{5}$$

where $\boldsymbol{K}_{\tilde{\mathcal{G}}_0}$ is an n-by-n covariance matrix with its (i, j)th entry being $k_{\tilde{\mathcal{G}}_0}(\boldsymbol{u}^{(i)}, \boldsymbol{u}^{(j)})$.

2.1.3. Posterior distributions

Conditional on the data $\boldsymbol{D}$, our current state of knowledge about $\mathcal{G}$ is expressed by its posterior distribution, which is also a GP:

$$\tilde{\mathcal{G}}_n(\boldsymbol{u}) \sim \mathcal{GP}(m_{\tilde{\mathcal{G}}_n}(\boldsymbol{u}), k_{\tilde{\mathcal{G}}_n}(\boldsymbol{u},\boldsymbol{u}')), \tag{6}$$

where $\tilde{\mathcal{G}}_n$ represents the posterior distribution of $\mathcal{G}$ after seeing n observations; $m_{\tilde{\mathcal{G}}_n}(\boldsymbol{u})$ and $k_{\tilde{\mathcal{G}}_n}(\boldsymbol{u},\boldsymbol{u}')$ are the posterior mean and covariance functions respectively, which can be expressed as:

$$m_{\tilde{\mathcal{G}}_n}(\boldsymbol{u}) = m_{\tilde{\mathcal{G}}_0}(\boldsymbol{u}) + \boldsymbol{k}_{\tilde{\mathcal{G}}_0}(\boldsymbol{u},\boldsymbol{\mathcal{U}})\boldsymbol{K}_{\tilde{\mathcal{G}}_0}^{-1}\left(\boldsymbol{\mathcal{Y}} - \boldsymbol{m}_{\tilde{\mathcal{G}}_0}(\boldsymbol{\mathcal{U}})\right), \tag{7}$$

$$k_{\tilde{\mathcal{G}}_n}(\boldsymbol{u},\boldsymbol{u}') = k_{\tilde{\mathcal{G}}_0}(\boldsymbol{u},\boldsymbol{u}') - \boldsymbol{k}_{\tilde{\mathcal{G}}_0}(\boldsymbol{u},\boldsymbol{\mathcal{U}})\boldsymbol{K}_{\tilde{\mathcal{G}}_0}^{-1}\boldsymbol{k}_{\tilde{\mathcal{G}}_0}(\boldsymbol{\mathcal{U}},\boldsymbol{u}'), \tag{8}$$

where $\boldsymbol{m}_{\tilde{\mathcal{G}}_0}(\boldsymbol{\mathcal{U}})$ is an n-by-1 column vector with its i-the element being $m_{\tilde{\mathcal{G}}_0}(\boldsymbol{u}^{(i)})$; $\boldsymbol{k}_{\tilde{\mathcal{G}}_0}(\boldsymbol{u},\boldsymbol{\mathcal{U}})$ is a 1-by-n row vector with its ith element being $k_{\tilde{\mathcal{G}}_0}(\boldsymbol{u},\boldsymbol{u}^{(i)})$; $\boldsymbol{k}_{\tilde{\mathcal{G}}_0}(\boldsymbol{\mathcal{U}},\boldsymbol{u}')$ is an n-by-1 column vector with its ith element being $k_{\tilde{\mathcal{G}}_0}(\boldsymbol{u}^{(i)},\boldsymbol{u}')$.

The posterior distribution of the indicator function $\mathcal{I}$ conditional on $\boldsymbol{D}$ follows a generalized Bernoulli process (GBP):

$$\tilde{\mathcal{I}}_n(\boldsymbol{u}) \sim \mathcal{GBP}(m_{\tilde{\mathcal{I}}_n}(\boldsymbol{u}), k_{\tilde{\mathcal{I}}_n}(\boldsymbol{u},\boldsymbol{u}')), \tag{9}$$

where $\tilde{\mathcal{I}}_n$ denotes the posterior distribution of $\mathcal{I}$; $m_{\tilde{\mathcal{I}}_n}(\boldsymbol{u})$ and $k_{\tilde{\mathcal{I}}_n}(\boldsymbol{u},\boldsymbol{u}')$ are the posterior mean and covariance functions respectively, which can be given by:

$$m_{\tilde{\mathcal{I}}_n}(\boldsymbol{u}) = \boldsymbol{\Phi}\left(-\frac{m_{\tilde{\mathcal{G}}_n}(\boldsymbol{u})}{\sigma_{\tilde{\mathcal{G}}_n}(\boldsymbol{u})}\right), \tag{10}$$

$$\begin{aligned} k_{\tilde{\mathcal{I}}_n}(\boldsymbol{u},\boldsymbol{u}') = {} & \boldsymbol{\Phi}_2\left(\begin{bmatrix}0\\0\end{bmatrix}; \begin{bmatrix} m_{\tilde{\mathcal{G}}_n}(\boldsymbol{u}) \\ m_{\tilde{\mathcal{G}}_n}(\boldsymbol{u}')\end{bmatrix}, \begin{bmatrix} \sigma^2_{\tilde{\mathcal{G}}_n}(\boldsymbol{u}) & k_{\tilde{\mathcal{G}}_n}(\boldsymbol{u}',\boldsymbol{u}) \\ k_{\tilde{\mathcal{G}}_n}(\boldsymbol{u},\boldsymbol{u}') & \sigma^2_{\tilde{\mathcal{G}}_n}(\boldsymbol{u}')\end{bmatrix}\right) \\ & - \boldsymbol{\Phi}\left(-\frac{m_{\tilde{\mathcal{G}}_n}(\boldsymbol{u})}{\sigma_{\tilde{\mathcal{G}}_n}(\boldsymbol{u})}\right)\boldsymbol{\Phi}\left(-\frac{m_{\tilde{\mathcal{G}}_n}(\boldsymbol{u}')}{\sigma_{\tilde{\mathcal{G}}_n}(\boldsymbol{u}')}\right), \end{aligned} \tag{11}$$

where $\boldsymbol{\Phi}$ denotes the cumulative distribution function (CDF) of a standard normal variable; $\boldsymbol{\Phi}_2$ denotes the bi-variate normal CDF, which has no analytical solution; $\sigma_{\tilde{\mathcal{G}}_n}(\boldsymbol{u})$ is the posterior standard deviation function of $\mathcal{G}$, i.e., $\sigma_{\tilde{\mathcal{G}}_n}(\boldsymbol{u}) = \sqrt{k_{\tilde{\mathcal{G}}_n}(\boldsymbol{u},\boldsymbol{u})}$.

The distribution type of the posterior failure probability $\tilde{\mathcal{P}}_{f,n}$ is not known exactly. Fortunately, its posterior mean and variance are available:

$$m_{\tilde{\mathcal{P}}_{f,n}} = \int_{\mathcal{U}} \boldsymbol{\Phi}\left(-\frac{m_{\tilde{\mathcal{G}}_n}(\boldsymbol{u})}{\sigma_{\tilde{\mathcal{G}}_n}(\boldsymbol{u})}\right)\phi(\boldsymbol{u})\mathrm{d}\boldsymbol{u}, \tag{12}$$

$$\sigma^2_{\tilde{\mathcal{P}}_{f,n}} = \int_{\mathcal{U}}\int_{\mathcal{U}} k_{\tilde{\mathcal{I}}_n}(\boldsymbol{u},\boldsymbol{u}')\phi(\boldsymbol{u})\phi(\boldsymbol{u}')\mathrm{d}\boldsymbol{u}\mathrm{d}\boldsymbol{u}', \tag{13}$$

where ϕ denotes the joint PDF of $\boldsymbol{U}$; $k_{\tilde{\mathcal{I}}_n}(\boldsymbol{u},\boldsymbol{u}')$ is defined in Eq. (11). Once $\boldsymbol{D}$ is given, the posterior mean $m_{\tilde{\mathcal{P}}_{f,n}}$ naturally serves as a point estimate of the failure probability. More importantly, the posterior variance $\sigma^2_{\tilde{\mathcal{P}}_{f,n}}$ can measure our epistemic uncertainty in the estimate due to the finite (more often limited) number of $\mathcal{G}$-function observations. However, both $m_{\tilde{\mathcal{P}}_{f,n}}$ and $\sigma^2_{\tilde{\mathcal{P}}_{f,n}}$ are analytically intractable and entail numerical integration. Compared to $m_{\tilde{\mathcal{P}}_{f,n}}$, the calculation of $\sigma^2_{\tilde{\mathcal{P}}_{f,n}}$ is much more challenging due to its underlying complexity, making it difficult to use in the development of Bayesian active learning reliability analysis methods.

2.2. Typical Bayesian active learning reliability analysis methods

As mentioned earlier, some Bayesian active learning reliability analysis methods have already been developed, which are based on, or can be seen as based on the BFPI framework. Typical methods include the ALPI [29], PBALC [32], SBALQ [33], PBPI [34] and QBALC [35]. The stopping criteria and learning functions developed in these methods are summarized in Table 1. It should be noted that all the stopping criteria entail numerical integration, which is not detailed here. Furthermore, some of the methods allow for the selection of multiple points from the learning functions, thus enabling parallel distributed processing. Despite significant efforts, there remains room for the development of new reliability analysis methods based on the BFPI framework that can further reduce the number of performance function calls while maintaining a desired level of accuracy.

3. Weakly Bayesian active learning quadrature

In this section, we present another novel Bayesian active learning method called WBALQ for structural reliability analysis with extremely small failure probabilities, which is based on the BFPI framework. The main innovation of our method lies in the development of the stopping criterion and learning function by properly exploiting the posterior statistics of the failure probability. Since the posterior variance is computationally demanding, we try to avoid using it directly as existing Bayesian active learning reliability analysis methods do. However, our method differs significantly from these existing methods in the way we construct the stopping criterion and the learning function, as described below. Note that the proposed method is called 'Weakly' Bayesian active learning because it does not fully incorporate all the Bayesian aspects of the BFPI framework.

3.1. Stopping criterion and its numerical treatment

It is often required when performing structural reliability analysis that the failure probability estimate maintains a certain level of accuracy. Therefore, our objective here is to devise a stopping criterion that can assess the accuracy of the failure probability estimate, specifically the posterior mean (Eq. (12)), without depending on the posterior variance (Eq. (13)). To accomplish this, the key lies in developing an alternative measure capable of capturing our epistemic uncertainty about the failure probability. Moreover, this measure should be easier to compute than the posterior variance.

Let us examine the first absolute central moment (also known as mean absolute deviation around the mean) of the posterior failure probability $\tilde{\mathcal{P}}_{f,n}$:

$$\begin{aligned} & \mathbb{E}_{\tilde{\mathcal{P}}_{f,n}}\left\{\left|\tilde{\mathcal{P}}_{f,n} - m_{\tilde{\mathcal{P}}_{f,n}}\right|\right\} \\ & = \mathbb{E}_{\tilde{\mathcal{I}}_n}\left\{\left|\int_{\mathcal{U}} \tilde{\mathcal{I}}_n(\boldsymbol{u})\,\phi(\boldsymbol{u})\mathrm{d}\boldsymbol{u} - \int_{\mathcal{U}} \boldsymbol{\Phi}\left(-\frac{m_{\tilde{\mathcal{G}}_n}(\boldsymbol{u})}{\sigma_{\tilde{\mathcal{G}}_n}(\boldsymbol{u})}\right)\phi(\boldsymbol{u})\mathrm{d}\boldsymbol{u}\right|\right\} \\ & = \mathbb{E}_{\tilde{\mathcal{I}}_n}\left\{\left|\int_{\mathcal{U}} \left[\tilde{\mathcal{I}}_n(\boldsymbol{u}) - \boldsymbol{\Phi}\left(-\frac{m_{\tilde{\mathcal{G}}_n}(\boldsymbol{u})}{\sigma_{\tilde{\mathcal{G}}_n}(\boldsymbol{u})}\right)\right]\phi(\boldsymbol{u})\mathrm{d}\boldsymbol{u}\right|\right\} \\ & \le \mathbb{E}_{\tilde{\mathcal{I}}_n}\left\{\int_{\mathcal{U}} \left|\tilde{\mathcal{I}}_n(\boldsymbol{u}) - \boldsymbol{\Phi}\left(-\frac{m_{\tilde{\mathcal{G}}_n}(\boldsymbol{u})}{\sigma_{\tilde{\mathcal{G}}_n}(\boldsymbol{u})}\right)\right|\phi(\boldsymbol{u})\mathrm{d}\boldsymbol{u}\right\} \\ & = \int_{\mathcal{U}} \mathbb{E}_{\tilde{\mathcal{I}}_n}\left\{\left|\tilde{\mathcal{I}}_n(\boldsymbol{u}) - \boldsymbol{\Phi}\left(-\frac{m_{\tilde{\mathcal{G}}_n}(\boldsymbol{u})}{\sigma_{\tilde{\mathcal{G}}_n}(\boldsymbol{u})}\right)\right|\right\}\phi(\boldsymbol{u})\mathrm{d}\boldsymbol{u} \\ & = \int_{\mathcal{U}} \left[\left|0 - \boldsymbol{\Phi}\left(-\frac{m_{\tilde{\mathcal{G}}_n}(\boldsymbol{u})}{\sigma_{\tilde{\mathcal{G}}_n}(\boldsymbol{u})}\right)\right| \times \boldsymbol{\Phi}\left(\frac{m_{\tilde{\mathcal{G}}_n}(\boldsymbol{u})}{\sigma_{\tilde{\mathcal{G}}_n}(\boldsymbol{u})}\right) + \left|1 - \boldsymbol{\Phi}\left(-\frac{m_{\tilde{\mathcal{G}}_n}(\boldsymbol{u})}{\sigma_{\tilde{\mathcal{G}}_n}(\boldsymbol{u})}\right)\right| \right. \\ & \quad \left. \times\, \boldsymbol{\Phi}\left(-\frac{m_{\tilde{\mathcal{G}}_n}(\boldsymbol{u})}{\sigma_{\tilde{\mathcal{G}}_n}(\boldsymbol{u})}\right)\right]\phi(\boldsymbol{u})\mathrm{d}\boldsymbol{u} \\ & = 2\int_{\mathcal{U}} \boldsymbol{\Phi}\left(-\frac{m_{\tilde{\mathcal{G}}_n}(\boldsymbol{u})}{\sigma_{\tilde{\mathcal{G}}_n}(\boldsymbol{u})}\right)\boldsymbol{\Phi}\left(\frac{m_{\tilde{\mathcal{G}}_n}(\boldsymbol{u})}{\sigma_{\tilde{\mathcal{G}}_n}(\boldsymbol{u})}\right)\phi(\boldsymbol{u})\mathrm{d}\boldsymbol{u}, \end{aligned} \tag{14}$$

where $\mathbb{E}_A\{B\}$ means to take expectation of B with respect to A. If we denote

$$\lambda_{\tilde{\mathcal{I}}_n} = \int_{\mathcal{U}} \boldsymbol{\Phi}\left(-\frac{m_{\tilde{\mathcal{G}}_n}(\boldsymbol{u})}{\sigma_{\tilde{\mathcal{G}}_n}(\boldsymbol{u})}\right)\boldsymbol{\Phi}\left(\frac{m_{\tilde{\mathcal{G}}_n}(\boldsymbol{u})}{\sigma_{\tilde{\mathcal{G}}_n}(\boldsymbol{u})}\right)\phi(\boldsymbol{u})\mathrm{d}\boldsymbol{u}, \tag{15}$$

then there exists

$$\mathbb{E}_{\tilde{\mathcal{P}}_{f,n}}\left\{\left|\tilde{\mathcal{P}}_{f,n} - m_{\tilde{\mathcal{P}}_{f,n}}\right|\right\} \le 2\lambda_{\tilde{\mathcal{I}}_n}. \tag{16}$$

Table 1
Stopping criteria and learning functions developed in several typical Bayesian active learning reliability analysis methods.

Method	Stopping criterion	Learning function
ALPI	$\frac{\int_{\mathcal{U}}\sqrt{\Phi\left(-\frac{m_{\hat{\mathcal{G}}_n}(\boldsymbol{u})}{\sigma_{\hat{\mathcal{G}}_n}(\boldsymbol{u})}\right)\Phi\left(\frac{m_{\hat{\mathcal{G}}_n}(\boldsymbol{u})}{\sigma_{\hat{\mathcal{G}}_n}(\boldsymbol{u})}\right)}\phi(\boldsymbol{u})\mathrm{d}\boldsymbol{u}}{\int_{\mathcal{U}}\Phi\left(-\frac{m_{\hat{\mathcal{G}}_n}(\boldsymbol{u})}{\sigma_{\hat{\mathcal{G}}_n}(\boldsymbol{u})}\right)\phi(\boldsymbol{u})\mathrm{d}\boldsymbol{u}}<\epsilon$	$\mathrm{LF}(\boldsymbol{u})=\sqrt{\Phi\left(-\frac{m_{\hat{\mathcal{G}}_n}(\boldsymbol{u})}{\sigma_{\hat{\mathcal{G}}_n}(\boldsymbol{u})}\right)\Phi\left(\frac{m_{\hat{\mathcal{G}}_n}(\boldsymbol{u})}{\sigma_{\hat{\mathcal{G}}_n}(\boldsymbol{u})}\right)}\phi(\boldsymbol{u})$
PBALC1	$\frac{\int_{\mathcal{U}}\left[\Phi\left(-\frac{m_{\hat{\mathcal{G}}_n}(\boldsymbol{u})}{\sigma_{\hat{\mathcal{G}}_n}(\boldsymbol{u})}\right)-\Phi\left(-\frac{m_{\hat{\mathcal{G}}_n}(\boldsymbol{u})}{\sigma_{\hat{\mathcal{G}}_n}(\boldsymbol{u})}-b\right)\right]\phi(\boldsymbol{u})\mathrm{d}\boldsymbol{u}}{\int_{\mathcal{U}}\Phi\left(-\frac{m_{\hat{\mathcal{G}}_n}(\boldsymbol{u})}{\sigma_{\hat{\mathcal{G}}_n}(\boldsymbol{u})}\right)\phi(\boldsymbol{u})\mathrm{d}\boldsymbol{u}}<\epsilon_1$	$\mathrm{LF}(\boldsymbol{u})=\left[\Phi\left(-\frac{m_{\hat{\mathcal{G}}_n}(\boldsymbol{u})}{\sigma_{\hat{\mathcal{G}}_n}(\boldsymbol{u})}\right)-\Phi\left(-\frac{m_{\hat{\mathcal{G}}_n}(\boldsymbol{u})}{\sigma_{\hat{\mathcal{G}}_n}(\boldsymbol{u})}-b\right)\right]\phi(\boldsymbol{u})$
PBALC2	$\frac{\int_{\mathcal{U}}\left[\Phi\left(-\frac{m_{\hat{\mathcal{G}}_n}(\boldsymbol{u})}{\sigma_{\hat{\mathcal{G}}_n}(\boldsymbol{u})}+b\right)-\Phi\left(-\frac{m_{\hat{\mathcal{G}}_n}(\boldsymbol{u})}{\sigma_{\hat{\mathcal{G}}_n}(\boldsymbol{u})}\right)\right]\phi(\boldsymbol{u})\mathrm{d}\boldsymbol{u}}{\int_{\mathcal{U}}\Phi\left(-\frac{m_{\hat{\mathcal{G}}_n}(\boldsymbol{u})}{\sigma_{\hat{\mathcal{G}}_n}(\boldsymbol{u})}\right)\phi(\boldsymbol{u})\mathrm{d}\boldsymbol{u}}<\epsilon_2$	$\mathrm{LF}(\boldsymbol{u})=\left[\Phi\left(-\frac{m_{\hat{\mathcal{G}}_n}(\boldsymbol{u})}{\sigma_{\hat{\mathcal{G}}_n}(\boldsymbol{u})}+b\right)-\Phi\left(-\frac{m_{\hat{\mathcal{G}}_n}(\boldsymbol{u})}{\sigma_{\hat{\mathcal{G}}_n}(\boldsymbol{u})}\right)\right]\phi(\boldsymbol{u})$
PBALC3	$\frac{\int_{\mathcal{U}}\left[\Phi\left(-\frac{m_{\hat{\mathcal{G}}_n}(\boldsymbol{u})}{\sigma_{\hat{\mathcal{G}}_n}(\boldsymbol{u})}+b\right)-\Phi\left(-\frac{m_{\hat{\mathcal{G}}_n}(\boldsymbol{u})}{\sigma_{\hat{\mathcal{G}}_n}(\boldsymbol{u})}-b\right)\right]\phi(\boldsymbol{u})\mathrm{d}\boldsymbol{u}}{\int_{\mathcal{U}}\Phi\left(-\frac{m_{\hat{\mathcal{G}}_n}(\boldsymbol{u})}{\sigma_{\hat{\mathcal{G}}_n}(\boldsymbol{u})}\right)\phi(\boldsymbol{u})\mathrm{d}\boldsymbol{u}}<\epsilon_3$	$\mathrm{LF}(\boldsymbol{u})=\left[\Phi\left(-\frac{m_{\hat{\mathcal{G}}_n}(\boldsymbol{u})}{\sigma_{\hat{\mathcal{G}}_n}(\boldsymbol{u})}+b\right)-\Phi\left(-\frac{m_{\hat{\mathcal{G}}_n}(\boldsymbol{u})}{\sigma_{\hat{\mathcal{G}}_n}(\boldsymbol{u})}-b\right)\right]\phi(\boldsymbol{u})$
SBALQ	$\frac{\int_{\mathcal{U}}\Phi\left(-\frac{\lvert m_{\hat{\mathcal{G}}_n}(\boldsymbol{u})\rvert}{\sigma_{\hat{\mathcal{G}}_n}(\boldsymbol{u})}\right)\phi(\boldsymbol{u})\mathrm{d}\boldsymbol{u}}{\int_{\mathcal{U}}\Phi\left(-\frac{m_{\hat{\mathcal{G}}_n}(\boldsymbol{u})}{\sigma_{\hat{\mathcal{G}}_n}(\boldsymbol{u})}\right)\phi(\boldsymbol{u})\mathrm{d}\boldsymbol{u}}<\epsilon$	$\mathrm{LF}(\boldsymbol{u})=\Phi\left(-\frac{\lvert m_{\hat{\mathcal{G}}_n}(\boldsymbol{u})\rvert}{\sigma_{\hat{\mathcal{G}}_n}(\boldsymbol{u})}\right)\phi(\boldsymbol{u})$
PBPI	$\frac{\int_{\mathcal{U}}\left[\Phi\left(-\frac{m_{\hat{\mathcal{G}}_n}(\boldsymbol{u})}{\sigma_{\hat{\mathcal{G}}_n}(\boldsymbol{u})}\right)\Phi\left(\frac{m_{\hat{\mathcal{G}}_n}(\boldsymbol{u})}{\sigma_{\hat{\mathcal{G}}_n}(\boldsymbol{u})}\right)\right]^{\frac{a}{2}}\phi(\boldsymbol{u})\mathrm{d}\boldsymbol{u}}{\int_{\mathcal{U}}\Phi\left(-\frac{m_{\hat{\mathcal{G}}_n}(\boldsymbol{u})}{\sigma_{\hat{\mathcal{G}}_n}(\boldsymbol{u})}\right)\phi(\boldsymbol{u})\mathrm{d}\boldsymbol{u}}<\epsilon$	$\mathrm{LF}(\boldsymbol{u})=\left[\Phi\left(-\frac{m_{\hat{\mathcal{G}}_n}(\boldsymbol{u})}{\sigma_{\hat{\mathcal{G}}_n}(\boldsymbol{u})}\right)\Phi\left(\frac{m_{\hat{\mathcal{G}}_n}(\boldsymbol{u})}{\sigma_{\hat{\mathcal{G}}_n}(\boldsymbol{u})}\right)\right]^{\frac{a}{2}}$
QBALC	$\frac{\sqrt{\tilde{\rho}}\int_{\mathcal{U}}\sqrt{\Phi\left(-\frac{m_{\hat{\mathcal{G}}_n}(\boldsymbol{u})}{\sigma_{\hat{\mathcal{G}}_n}(\boldsymbol{u})}\right)\Phi\left(\frac{m_{\hat{\mathcal{G}}_n}(\boldsymbol{u})}{\sigma_{\hat{\mathcal{G}}_n}(\boldsymbol{u})}\right)}\phi(\boldsymbol{u})\mathrm{d}\boldsymbol{u}}{\int_{\mathcal{U}}\Phi\left(-\frac{m_{\hat{\mathcal{G}}_n}(\boldsymbol{u})}{\sigma_{\hat{\mathcal{G}}_n}(\boldsymbol{u})}\right)\phi(\boldsymbol{u})\mathrm{d}\boldsymbol{u}}<\epsilon$	$\mathrm{LF}(\boldsymbol{u};p)=\sqrt{\Phi\left(-\frac{m_{\hat{\mathcal{G}}_n}(\boldsymbol{u})}{p\sigma_{\hat{\mathcal{G}}_n}(\boldsymbol{u})}\right)\Phi\left(\frac{m_{\hat{\mathcal{G}}_n}(\boldsymbol{u})}{p\sigma_{\hat{\mathcal{G}}_n}(\boldsymbol{u})}\right)}\phi(\boldsymbol{u})$

Note: ϵ, ϵ_1, ϵ_2 and ϵ_3 denotes the user-defined stopping criterion thresholds; b is a critical value that determines the desired credible level; α is a parameter; $\tilde{\rho}$ is the equivalent correlation coefficient; p is a penalty factor.

This indicates that the mean absolute deviation around the mean of the posterior failure probability $\tilde{P}_{f,n}$ has an upper bound of $2\lambda_{\tilde{I}_n}$. Note that when $\lambda_{\tilde{I}_n}$ approaches to zero, $\tilde{P}_{f,n}$ theoretically converges to the true failure probability. Thus, $\lambda_{\tilde{I}_n}$ can be considered as an alternative measure of the epistemic uncertainty in the failure probability. Besides, this measure is much easier to evaluate than the posterior variance $\sigma^2_{\tilde{P}_{f,n}}$. Interestingly, $\lambda_{\tilde{I}_n}$ happens to be the integrated posterior variance $\sigma^2_{\tilde{I}_n}(\boldsymbol{u})$ under the weight $\phi(\boldsymbol{u})$, and also a special case of the pseudo posterior standard deviation given in [34]. It is worth mentioning that a looser upper bound of $\mathbb{E}_{\tilde{P}_{f,n}}\left\{\left|\tilde{P}_{f,n}-m_{\tilde{P}_{f,n}}\right|\right\}$ was provided in a previous study [36].

Once the new measure $\lambda_{\tilde{I}_n}$ has been obtained, the stopping criterion is defined as follows:

$$\frac{\lambda_{\tilde{I}_n}}{m_{\tilde{P}_{f,n}}}<\epsilon, \tag{17}$$

where ϵ is a user-defined threshold, a small positive value of which is desired. The stopping criterion implies that the iterative process involved in the proposed method should stop as soon as $\lambda_{\tilde{I}n}$ becomes relatively small compared to $m_{\tilde{P}_{f,n}}$. Note that the proposed stopping criterion can be seen as a special case of the stopping criterion given in [34]. Since both $m_{\tilde{P}_{f,n}}$ and $\lambda_{\tilde{I}_n}$ lack analytical tractability, implementing the proposed stopping criterion necessitates the use of an effective numerical integration technique. In this study, we employ the 'Hyper-shell Simulation' (HSS) method developed in [33].

The standard normal space $\mathcal{U}$ is partitioned into h concentric hyper-spherical shells such that [37]:

$$\bigcup_{i=1}^{h}\mathcal{U}_i=\mathcal{U}, \tag{18}$$

$$\mathcal{U}_i\bigcap\mathcal{U}_j=\emptyset, i\neq j, \tag{19}$$

where $\mathcal{U}_i=\left\{\boldsymbol{u}|R_{i-1}\leq\|\boldsymbol{u}\|<R_i\right\}$ is the ith shell, defined by the inter radius R_{i-1} and outer radius R_i. The sequence of radii $\left\{R_i\right\}_{i=0}^{h}$ is in ascending order such that $0=R_0<R_1<\cdots<R_h=\infty$. As suggested by [37], the radius R_i $(i=1,2,\ldots,h-1)$ can be specified as $R_i=\sqrt{\chi_d^{-2}(1-10^{-i})}$, where $\chi_d^{-2}(\cdot)$ represents the inverse CDF of the chi-squared distribution with degree d. One can refer to Fig. 1(a) for a schematic illustration of the space partition in three dimensions.

Following the standard normal space decomposition, $m_{\tilde{P}_{f,n}}$ and $\lambda_{\tilde{I}_n}$ can be further expressed as:

$$\begin{aligned}
m_{\tilde{P}_{f,n}}&=\sum_{i=1}^{h}m^{(i)}_{\tilde{P}_{f,n}}\\
&=\sum_{i=1}^{h}\int_{\mathcal{U}_i}\Phi\left(-\frac{m_{\tilde{\mathcal{G}}_n}(\boldsymbol{u})}{\sigma_{\tilde{\mathcal{G}}_n}(\boldsymbol{u})}\right)\phi(\boldsymbol{u})\mathrm{d}\boldsymbol{u}\\
&=\sum_{i=1}^{h-1}v_i\int_{\mathcal{U}_i}\Phi\left(-\frac{m_{\tilde{\mathcal{G}}_n}(\boldsymbol{u})}{\sigma_{\tilde{\mathcal{G}}_n}(\boldsymbol{u})}\right)\phi(\boldsymbol{u})p^{(i)}(\boldsymbol{u})\mathrm{d}\boldsymbol{u}\\
&\quad+\delta_h\int_{\mathcal{U}_h}\Phi\left(-\frac{m_{\tilde{\mathcal{G}}_n}(\boldsymbol{u})}{\sigma_{\tilde{\mathcal{G}}_n}(\boldsymbol{u})}\right)\psi^{(h)}(\boldsymbol{u})\mathrm{d}\boldsymbol{u},
\end{aligned} \tag{20}$$

$$\begin{aligned}
\lambda_{\tilde{I}_n}&=\sum_{i=1}^{h}\lambda^{(i)}_{\tilde{I}_n}\\
&=\sum_{i=1}^{h}\int_{\mathcal{U}_i}\Phi\left(-\frac{m_{\tilde{\mathcal{G}}_n}(\boldsymbol{u})}{\sigma_{\tilde{\mathcal{G}}_n}(\boldsymbol{u})}\right)\Phi\left(\frac{m_{\tilde{\mathcal{G}}_n}(\boldsymbol{u})}{\sigma_{\tilde{\mathcal{G}}_n}(\boldsymbol{u})}\right)\phi(\boldsymbol{u})\mathrm{d}\boldsymbol{u}\\
&=\sum_{i=1}^{h-1}v_i\int_{\mathcal{U}_i}\Phi\left(-\frac{m_{\tilde{\mathcal{G}}_n}(\boldsymbol{u})}{\sigma_{\tilde{\mathcal{G}}_n}(\boldsymbol{u})}\right)\Phi\left(\frac{m_{\tilde{\mathcal{G}}_n}(\boldsymbol{u})}{\sigma_{\tilde{\mathcal{G}}_n}(\boldsymbol{u})}\right)\phi(\boldsymbol{u})p^{(i)}(\boldsymbol{u})\mathrm{d}\boldsymbol{u}\\
&\quad+\delta_h\int_{\mathcal{U}_h}\Phi\left(-\frac{m_{\tilde{\mathcal{G}}_n}(\boldsymbol{u})}{\sigma_{\tilde{\mathcal{G}}_n}(\boldsymbol{u})}\right)\Phi\left(\frac{m_{\tilde{\mathcal{G}}_n}(\boldsymbol{u})}{\sigma_{\tilde{\mathcal{G}}_n}(\boldsymbol{u})}\right)\psi^{(h)}(\boldsymbol{u})\mathrm{d}\boldsymbol{u},
\end{aligned} \tag{21}$$

where $p^{(i)}(\boldsymbol{u})$ denotes the uniform sampling PDF for the $h-1$ inner hyper-shells:

$$p^{(i)}(\boldsymbol{u})=\begin{cases}\frac{1}{v_i},\boldsymbol{u}\in\mathcal{U}_i,i=1,2,\ldots,h-1\\0,\text{otherwise}\end{cases}, \tag{22}$$

in which v_i denotes the volume of the ith hyper-shell, given by $v_i=\frac{\pi^{d/2}}{\Gamma(d/2+1)}\left(R_i^d-R_{i-1}^d\right)$ with $\Gamma(\cdot)$ being Euler's gamma function; $\psi^{(h)}(\boldsymbol{u})$ denotes truncated normal sampling PDF for the outermost hyper-shell:

$$\psi^{(h)}(\boldsymbol{u})=\begin{cases}\frac{\phi(\boldsymbol{u})}{\delta_h},\boldsymbol{u}\in\mathcal{U}_h\\0,\text{otherwise}\end{cases}, \tag{23}$$

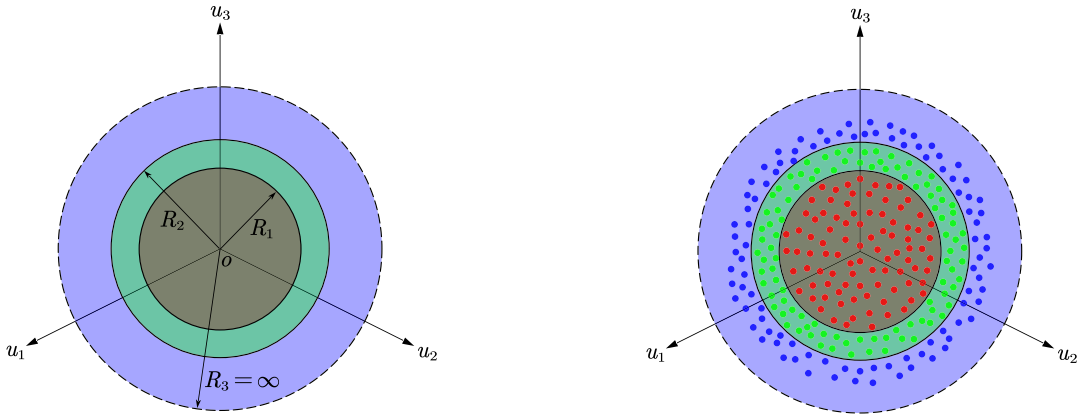

(a) Space partition (b) Subdomain sampling

Fig. 1. Schematic illustration of the HSS method ($h = 3$) in three dimensions.

in which $\delta_h = \int_{\mathcal{U}_h} \phi_U(\boldsymbol{u})\mathrm{d}\boldsymbol{u}$ is the probability content of the outermost hyper-shell $\mathcal{U}_h$.

The estimators of $m_{\bar{\mathcal{P}}_{f,n}}$ and $\lambda_{\bar{\mathcal{I}}_n}$ can be given by:

$$\begin{aligned}\hat{m}_{\bar{\mathcal{P}}_{f,n}} &= \sum_{i=1}^{h} \hat{m}^{(i)}_{\bar{\mathcal{P}}_{f,n}} \\ &= \sum_{i=1}^{h-1} v_i \left[\frac{1}{N_i}\sum_{j=1}^{N_i} \boldsymbol{\Phi}\left(-\frac{m_{\tilde{\mathcal{G}}_n}(\boldsymbol{u}^{(i,j)})}{\sigma_{\tilde{\mathcal{G}}_n}(\boldsymbol{u}^{(i,j)})}\right)\phi(\boldsymbol{u}^{(i,j)})\right] \\ &\quad + \delta_h \frac{1}{N_h}\sum_{j=1}^{N_h} \boldsymbol{\Phi}\left(-\frac{m_{\tilde{\mathcal{G}}_n}(\boldsymbol{u}^{(h,j)})}{\sigma_{\tilde{\mathcal{G}}_n}(\boldsymbol{u}^{(h,j)})}\right),\end{aligned} \tag{24}$$

$$\begin{aligned}\hat{\lambda}_{\bar{\mathcal{I}}_n} &= \sum_{i=1}^{h-1} \hat{\lambda}^{(i)}_{\bar{\mathcal{I}}_n} \\ &= \sum_{i=1}^{h-1} v_i \left[\frac{1}{N_i}\sum_{j=1}^{N_i} \boldsymbol{\Phi}\left(-\frac{m_{\tilde{\mathcal{G}}_n}(\boldsymbol{u}^{(i,j)})}{\sigma_{\tilde{\mathcal{G}}_n}(\boldsymbol{u}^{(i,j)})}\right)\boldsymbol{\Phi}\left(\frac{m_{\tilde{\mathcal{G}}_n}(\boldsymbol{u}^{(i,j)})}{\sigma_{\tilde{\mathcal{G}}_n}(\boldsymbol{u}^{(i,j)})}\right)\phi(\boldsymbol{u}^{(i,j)})\right] \\ &\quad + \delta_h \frac{1}{N_h}\sum_{j=1}^{N_h} \boldsymbol{\Phi}\left(-\frac{m_{\tilde{\mathcal{G}}_n}(\boldsymbol{u}^{(h,j)})}{\sigma_{\tilde{\mathcal{G}}_n}(\boldsymbol{u}^{(h,j)})}\right)\boldsymbol{\Phi}\left(\frac{m_{\tilde{\mathcal{G}}_n}(\boldsymbol{u}^{(h,j)})}{\sigma_{\tilde{\mathcal{G}}_n}(\boldsymbol{u}^{(h,j)})}\right),\end{aligned} \tag{25}$$

where $\{\boldsymbol{u}^{(i,j)}\}_{j=1}^{N_i}$ is a set of N_i random samples drawn from $p^{(i)}(\boldsymbol{u})$, $i = 1, 2, \ldots, h-1$; $\{\boldsymbol{u}^{(h,j)}\}_{j=1}^{N_h}$ is a set of N_h random samples generated according to $\psi^{(h)}(\boldsymbol{u})$. For details on how to obtain these samples, the reader is referred to [33]. See Fig. 1(b) for a schematic illustration of the sub-region sampling in three dimensions. The terms "partial means" and "total means" will be used to refer to the quantities $\hat{m}^{(i)}_{\bar{\mathcal{P}}_{f,n}}$ and $\hat{\lambda}^{(i)}_{\bar{\mathcal{I}}_n}$, respectively, and to the quantities $\hat{m}_{\bar{\mathcal{P}}_{f,n}}$ and $\hat{\lambda}_{\bar{\mathcal{I}}_n}$, respectively.

The variances associated with $\hat{m}_{\bar{\mathcal{P}}_{f,n}}$ and $\hat{\lambda}_{\bar{\mathcal{I}}_n}$ are expressed as:

$$\begin{aligned}\mathbb{V}\left[\hat{m}_{\bar{\mathcal{P}}_{f,n}}\right] &= \sum_{i=1}^{h} \mathbb{V}\left[\hat{m}^{(i)}_{\bar{\mathcal{P}}_{f,n}}\right] \\ &= \sum_{i=1}^{h-1} \frac{1}{N_i - 1}\left\{\frac{1}{N_i}\sum_{j=1}^{N_i}\left[v_i \boldsymbol{\Phi}\left(-\frac{m_{\tilde{\mathcal{G}}_n}(\boldsymbol{u}^{(i,j)})}{\sigma_{\tilde{\mathcal{G}}_n}(\boldsymbol{u}^{(i,j)})}\right)\phi(\boldsymbol{u}^{(i,j)})\right]^2 - \hat{m}^{(i),2}_{\bar{\mathcal{P}}_{f,n}}\right\} \\ &\quad + \frac{1}{N_h - 1}\left\{\frac{1}{N_h}\sum_{j=1}^{N_h}\left[\delta_h \boldsymbol{\Phi}\left(-\frac{m_{\tilde{\mathcal{G}}_n}(\boldsymbol{u}^{(h,j)})}{\sigma_{\tilde{\mathcal{G}}_n}(\boldsymbol{u}^{(h,j)})}\right)\right]^2 - \hat{m}^{(h),2}_{\bar{\mathcal{P}}_{f,n}}\right\},\end{aligned} \tag{26}$$

$$\begin{aligned}\mathbb{V}\left[\hat{\lambda}_{\bar{\mathcal{I}}_n}\right] &= \sum_{i=1}^{h} \mathbb{V}\left[\hat{\lambda}^{(i)}_{\bar{\mathcal{I}}_n}\right] \\ &= \sum_{i=1}^{h-1} \frac{1}{N_i - 1}\left\{\frac{1}{N_i}\sum_{j=1}^{N_i}\left[v_i \boldsymbol{\Phi}\left(-\frac{m_{\tilde{\mathcal{G}}_n}(\boldsymbol{u}^{(i,j)})}{\sigma_{\tilde{\mathcal{G}}_n}(\boldsymbol{u}^{(i,j)})}\right)\boldsymbol{\Phi}\left(\frac{m_{\tilde{\mathcal{G}}_n}(\boldsymbol{u}^{(i,j)})}{\sigma_{\tilde{\mathcal{G}}_n}(\boldsymbol{u}^{(i,j)})}\right)\phi(\boldsymbol{u}^{(i,j)})\right]^2 - \hat{\lambda}^{(i),2}_{\bar{\mathcal{I}}_n}\right\} \\ &\quad + \frac{1}{N_h - 1}\left\{\frac{1}{N_h}\sum_{j=1}^{N_h}\left[\delta_h \boldsymbol{\Phi}\left(-\frac{m_{\tilde{\mathcal{G}}_n}(\boldsymbol{u}^{(h,j)})}{\sigma_{\tilde{\mathcal{G}}_n}(\boldsymbol{u}^{(h,j)})}\right)\boldsymbol{\Phi}\left(\frac{m_{\tilde{\mathcal{G}}_n}(\boldsymbol{u}^{(h,j)})}{\sigma_{\tilde{\mathcal{G}}_n}(\boldsymbol{u}^{(h,j)})}\right)\right]^2 - \hat{\lambda}^{(h),2}_{\bar{\mathcal{I}}_n}\right\},\end{aligned} \tag{27}$$

where $\mathbb{V}[\cdot]$ means to take variance of its argument. We shall refer to $\mathbb{V}\left[\hat{m}^{(i)}_{\bar{\mathcal{P}}_{f,n}}\right]$ and $\mathbb{V}\left[\hat{\lambda}^{(i)}_{\bar{\mathcal{I}}_n}\right]$ as partial variances, and to $\mathbb{V}\left[\hat{m}_{\bar{\mathcal{P}}_{f,n}}\right]$ and $\mathbb{V}\left[\hat{\lambda}_{\bar{\mathcal{I}}_n}\right]$ total variances.

Clearly, the sample sizes for the different hyper-shells do not need to be identical. To effectively reduce the corresponding total variance, more samples should be allocated in the hyper-shell(s) with the largest partial variance(s). Therefore, it is recommended to increase the sample sizes progressively until a stopping criterion is met. This criterion is defined as $\sqrt{\mathbb{V}\left[\hat{m}_{\bar{\mathcal{P}}_{f,n}}\right]}/\hat{m}_{\bar{\mathcal{P}}_{f,n}} < \gamma_1$ and $\sqrt{\mathbb{V}\left[\hat{\lambda}_{\bar{\mathcal{I}}_n}\right]}/\hat{\lambda}_{\bar{\mathcal{I}}_n} < \gamma_2$, where γ_1 and γ_2 are two user-defined thresholds. For convenience, we assume that the sample size is the same for each enrichment in all hyper-shells, denoted as ΔN. Initially, ΔN samples for each hyper-shell are generated. Additional samples are only generated for the hyper-shell(s) with the largest partial variance(s) if the stopping criterion is not met. Note that the relatively time-consuming item $\boldsymbol{\Phi}\left(-\frac{m_{\tilde{\mathcal{G}}_n}(\boldsymbol{u})}{\sigma_{\tilde{\mathcal{G}}_n}(\boldsymbol{u})}\right)$ should be reused as much as possible to speed up the overall computation. For detailed information on the implementation of the HSS method, refer to [33]. The two terms involved in the proposed stopping criterion (InEq. (17)) should be replaced by their respective final estimates, i.e., $\hat{m}_{\bar{\mathcal{P}}_{f,n}}$ and $\hat{\lambda}_{\bar{\mathcal{I}}_n}$. The stopping criterion should be met two times in succession to increase its robustness.

3.2. Learning function and next best point selection

Another essential component of a Bayesian active learning reliability analysis method is the so-called learning function, which comes into

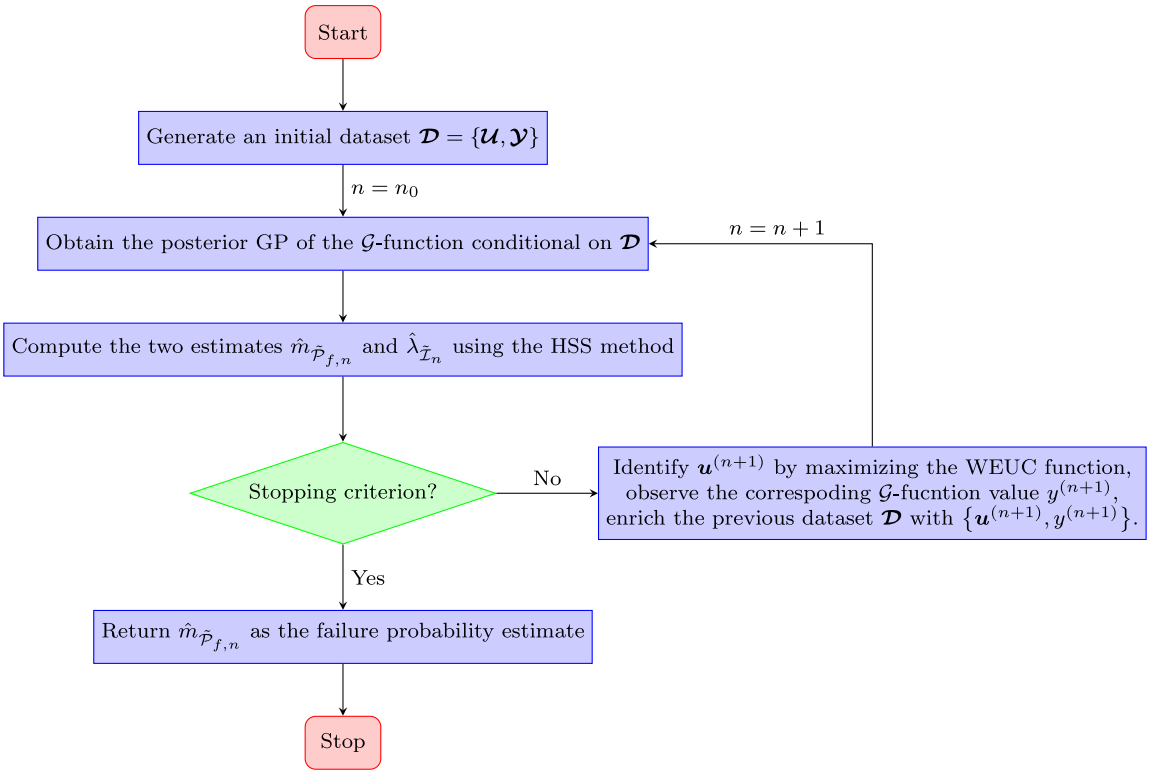

Fig. 2. Flowchart of the proposed WBALQ method.

play if the stopping criterion developed in the previous subsection is not met. Specifically, the learning function guides the learning process to identify the most promising point(s) at which to evaluate the $\mathcal{G}$-function next. Since we believe that the accuracy of failure probability estimate can be controlled by the stopping criterion (Ineq. (17)), a natural idea to design the sought learning function is to examine the term on the left-hand side of the inequality, i.e., the ratio of $\lambda_{\tilde{I}_n}$ and $m_{\tilde{\mathcal{P}}_{f,n}}$. This is not straightforward, however, mainly because it may be difficult to extract a unified function from the ratio involving two integrals. Alternatively, we might turn to $\lambda_{\tilde{I}_n}$, which serves as the epistemic uncertainty measure for the failure probability.

Following the idea above, we introduce a novel learning function termed 'Weighted Epistemic Uncertainty Contribution' (WEUC):

$$\mathrm{WEUC}(\boldsymbol{u}) = \underbrace{\sigma_{\tilde{\mathcal{G}}_n}(\boldsymbol{u})}_{①} \underbrace{\Phi\left(-\frac{m_{\tilde{\mathcal{G}}_n}(\boldsymbol{u})}{\sigma_{\tilde{\mathcal{G}}_n}(\boldsymbol{u})}\right)\Phi\left(\frac{m_{\tilde{\mathcal{G}}_n}(\boldsymbol{u})}{\sigma_{\tilde{\mathcal{G}}_n}(\boldsymbol{u})}\right)\phi(\boldsymbol{u})}_{②}, \tag{28}$$

where ① represents the posterior standard deviation function of $\mathcal{G}$, which serves as a weight for ②; ② is the integrand of $\lambda_{\tilde{I}_n}$, referred to as the 'epistemic uncertainty contribution'. The proposed WEUC function can be interpreted as follows. The second term ② actually provides a measure of the contribution of the epistemic uncertainty at point $\boldsymbol{u}$ to the total value of $\lambda_{\tilde{I}_n}$, which is then multiplied by the first term ① to reward points with large uncertainty (hence to increase the exploration).

The next best point to query the $\mathcal{G}$-function can be selected by:

$$\boldsymbol{u}^{(n+1)} = \underset{\boldsymbol{u}\in[-\beta,\beta]^d}{\arg\max}\, \mathrm{WEUC}(\boldsymbol{u}), \tag{29}$$

where $[-\beta,\beta]^d$ denotes a hyper-rectangle of side length β in the standard normal space $\mathcal{U}$; β can be determined according to $\beta = \sqrt{\chi_d^{-2}(1-\rho)}$ with $\rho = 1\times10^{-10}$ [32]. As the learning function is relatively cheap to evaluate, we can use any suitable meta-heuristic optimization algorithm to solve the optimization problem, such as the genetic algorithm.

3.3. Implementation procedure of the proposed method

The main procedure for implementing the proposed method is summarized below in six steps, together with a flowchart given in Fig. 2.

Step 1: Generating an initial dataset

First, a set of n_0 uniform samples $\mathcal{U} = \{\boldsymbol{u}^{(i)}\}_{i=1}^{n_0}$ is generated within a d-ball of radius R_0 using an appropriate low-discrepancy sequence. In this study, the radius R_0 is set to $R_0 = \sqrt{\chi_d^{-2}(1-\delta)}$ with $\delta = 1\times10^{-8}$, and the Hammersley sequence is employed. Subsequently, the output values of the $\mathcal{G}$-function at $\mathcal{U}$ can be evaluated, which are denoted as $\mathcal{Y} = \left[y^{(1)}, y^{(2)}, \ldots, y^{(n_0)}\right]^{\mathrm{T}}$ with $y^{(i)} = \mathcal{G}(\boldsymbol{u}^{(i)})$. At last, the initial dataset can be constructed as $\mathcal{D} = \{\mathcal{U}, \mathcal{Y}\}$. Let $n = n_0$.

Step 2: Obtaining the posterior statistics of $\mathcal{G}$

The posterior GP of the $\mathcal{G}$-function conditional on $\mathcal{D}$ needs to be acquired. This involves primarily estimating the hyperparameters using the maximum likelihood estimation method. In our study, we utilize the *fitrgp* function from the Statistics and Machine Learning Toolbox of MATLAB.

Step 3: Computing the two integral terms in the stopping criterion

One has to compute the two estimates $\hat{m}_{\tilde{\mathcal{P}}_{f,n}}$ and $\hat{\lambda}_{\tilde{I}_n}$ by using the HSS method outlined in Section 3.1.

Step 4: Checking the stopping criterion

If $\frac{\hat{\lambda}_{\tilde{I}_n}}{\hat{m}_{\tilde{\mathcal{P}}_{f,n}}} < \epsilon$ is satisfied twice in row, go to **Step 6**; Otherwise, proceed to **Step 5**.

Step 5: Enriching the dataset

First, the next best point $\boldsymbol{u}^{(n+1)}$ is identified by Eq. (29). Then, evaluating the $\mathcal{G}$ function at $\boldsymbol{u}^{(n+1)}$ gives its output value $y^{(n+1)}$. Finally, the previous dataset $\mathcal{D}$ is enriched with $\{\boldsymbol{u}^{(n+1)}, y^{(n+1)}\}$. Let $n = n+1$ and go to **Step 2**.

Step 6: Ending the algorithm

Return the last posterior mean estimate $\hat{m}_{\tilde{\mathcal{P}}_{f,n}}$ and end the algorithm.

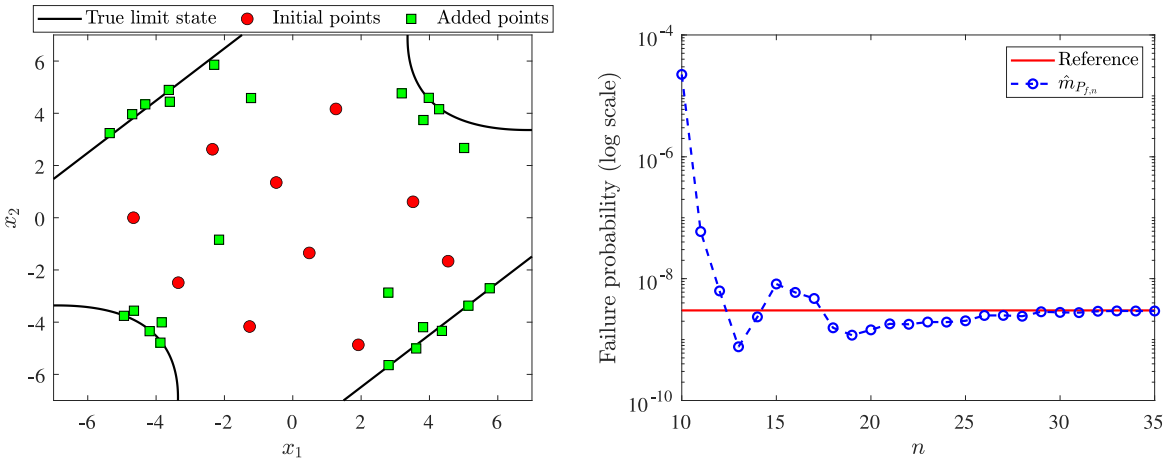

Fig. 3. Illustration of the proposed WBALQ method ($\epsilon = 3.0\%$) for Example 1.

4. Numerical examples

In this section, five numerical examples are examined to demonstrate the performance of the proposed WBALQ method in estimating extremely small failure probabilities. The parameters of our method are set as follows: $n_0 = 10$, $\Delta N = 10^5$, $h = 10$, $\gamma_1 = \gamma_2 = 2\%$, and ϵ is varied to see its effect. Where applicable, the failure probability estimate provided by MCS is used as the reference solution. In all the examples, the proposed method is compared with several other state-of-the-art methods: Active learning Kriging Markov Chain Monte Carlo (AK-MCMC) [38], PBALC1 [32], PBALC2 [32], PBALC3 [32], SBALQ [33], and QBALC [35]. To test their robustness, all the (Bayesian) active learning methods are run independently 20 times and the corresponding statistical results are reported.

4.1. Example 1: A series system with four branches

The first numerical example is concerned with a series system with four branches, which has been extensively studied (e.g., see [26]). The performance function is given by:

$$g(\boldsymbol{X}) = \min \begin{cases} a + \frac{(X_1 - X_2)^2}{10} - \frac{(X_1 + X_2)}{\sqrt{2}} \\ a + \frac{(X_1 - X_2)^2}{10} + \frac{(X + X_2)}{\sqrt{2}} \\ (X_1 - X_2) + \frac{b}{\sqrt{2}} \\ (X_2 - X_1) + \frac{b}{\sqrt{2}} \end{cases}, \tag{30}$$

where a and b are two constant parameters, which are specified as $a = 6$ and $b = 12$; X_1 and X_2 are two independent standard normal variables.

Table 2 reports the results of several methods, i.e., MCS, AK-MCMC, PBALC1, PBACL2, PBALC3, SBALQ, QBALC and the proposed WBALQ. The reference value for the failure probability is adopted as 3.01×10^{-9} (with a COV of 1.82%), produced by MCS with 10^{12} samples. At the cost of an average number of 195.45 performance function evaluations, AK-MCMC gives a biased mean value of the failure probability, i.e., 2.34×10^{-9}, with a rather large COV of 33.11%. PBALC1, PBALC2, PBALC3, SBALQ and QBALC perform well in terms of the number of g-function calls on average, as well as the unbiasedness and variability of the mean failure probability value. For the proposed WBALQ method itself, as the stopping criterion threshold ϵ decreases, (1) the number of performance function evaluations increases on average; (2) the bias of the mean failure probability value is reduced; (3) the COV of the mean failure probability value decreases. Taking the case $\epsilon = 3.0\%$ as an example, it is found that the proposed WBALQ method significantly outperforms AK-MCMC and slightly outperforms the other five methods (i.e., PBALC1, PBALC2, PBALC3, SBALQ, and QBALC) in terms of the average number of g-function calls.

Table 2
Reliability analysis results of Example 1 by several methods.

Method		N_{call}	$\hat{P}_f$	$\delta_{\hat{P}_f}$	Reference
MCS	–	10^{12}	3.01×10^{-9}	1.82%	[32]
AK-MCMC	–	195.45	2.34×10^{-9}	33.11%	[32]
PBALC1	$\epsilon_1 = 2.5\%$	44.75	3.04×10^{-9}	3.82%	[32]
PBALC2	$\epsilon_2 = 2.5\%$	50.10	3.04×10^{-9}	1.39%	[32]
PBALC3	$\epsilon_3 = 5.0\%$	49.50	3.03×10^{-9}	1.99%	[32]
SBALQ	$\epsilon = 2.0\%$	41.15	3.03×10^{-9}	1.31%	[33]
QBALC	$\epsilon = 5.0\%$	44.75	3.03×10^{-9}	2.57%	[35]
Proposed WBALQ	$\epsilon = 5.0\%$	32.05	2.79×10^{-9}	6.55%	–
	$\epsilon = 4.5\%$	33.50	2.85×10^{-9}	5.20%	–
	$\epsilon = 4.0\%$	34.30	2.91×10^{-9}	3.23%	–
	$\epsilon = 3.5\%$	35.20	2.95×10^{-9}	2.08%	–
	$\epsilon = 3.0\%$	36.00	2.98×10^{-9}	1.83%	–
	$\epsilon = 2.5\%$	37.10	2.99×10^{-9}	0.97%	–
	$\epsilon = 2.0\%$	39.05	3.01×10^{-9}	0.91%	–

Note: N_{call} = the total (average) number of G-function calls; $\hat{P}_f$ = the (mean) failure probability estimate; $\delta_{\hat{P}_f}$ = the COV of $\hat{P}_f$, which is obtained from 20 replications for (Bayesian) active learning methods.

The proposed method ($\epsilon = 3.0\%$) is further illustrated by Fig. 3 based on an arbitrary run. It can be seen from Fig. 3(a) that: (1) the initial 10 points are very scattered, as we expected; (2) most of the points identified in the active learning loop are located around the four branches of the true limit state curve. Fig. 3(b) shows that as the number of points increases, the posterior mean estimate of the failure probability eventually converges to the reference failure probability.

4.2. Example 2: A nonlinear oscillator

In the second example, we consider a single-degree-of-freedom nonlinear oscillator subject to a rectangular pulse load [20], as depicted in Fig. 4. The performance function is formulated as:

$$g(\boldsymbol{X}) = 3r - \left| \frac{2F_1}{c_1 + c_2} \sin\left(\frac{t_1}{2} \sqrt{\frac{c_1 + c_2}{m}} \right) \right|, \tag{31}$$

in which m, c_1, c_2, r, F_1 and t_1 are six basic random variables, as listed in Table 3.

The performance of the proposed WBALQ method is compared with several other methods (i.e., MCS, AK-MCMC, PBALC1, PBACL2, PBALC3, SBALQ and QBALC) in Table 4. The failure probability estimate given by MCS with 10^{12} samples is taken as the reference, which is 4.01×10^{-8} with a COV of 0.50%. AK-MCMC can provide an unbiased

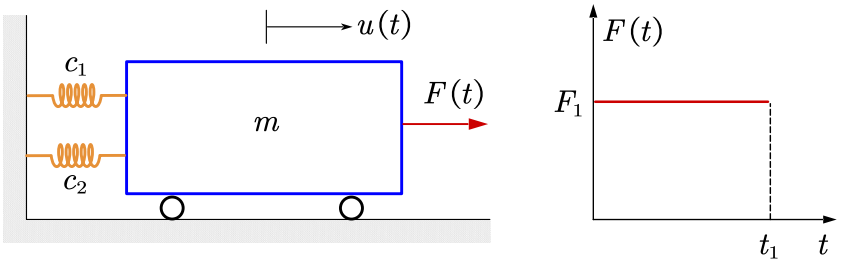

Fig. 4. A nonlinear oscillator subject to a rectangular pulse load.

Table 3
Basic random variables for Example 2.

Variable	Description	Distribution	Mean	COV
m	Mass	Lognormal	1.0	0.05
c_1	Stiffness	Lognormal	1.0	0.10
c_2	Stiffness	Lognormal	0.2	0.10
r	Yield displacement	Lognormal	0.5	0.10
F_1	Load amplitude	Lognormal	0.4	0.20
t_1	Load duration	Lognormal	1.0	0.20

Table 4
Reliability analysis results of Example 2 by several methods.

Method		N_{call}	$\hat{P}_f$	$\delta_{\hat{P}_f}$	Reference
MCS	–	10^{12}	4.01×10^{-8}	0.50%	[32]
AK-MCMC	–	282.30	4.03×10^{-8}	0.76%	[32]
PBALC1	$\epsilon_1 = 5.0\%$	29.10	4.03×10^{-8}	4.29%	[32]
PBALC2	$\epsilon_2 = 5.0\%$	31.90	4.07×10^{-8}	2.61%	[32]
PBALC3	$\epsilon_3 = 10.0\%$	30.95	4.05×10^{-8}	3.66%	[32]
SBALQ	$\epsilon = 4.0\%$	31.45	4.03×10^{-8}	1.72%	[33]
QBALC	$\epsilon = 5.0\%$	29.25	4.03×10^{-8}	2.49%	–
Proposed WBALQ	$\epsilon = 5.0\%$	24.00	3.95×10^{-8}	4.02%	–
	$\epsilon = 4.5\%$	25.25	3.99×10^{-8}	3.56%	–
	$\epsilon = 4.0\%$	26.20	3.99×10^{-8}	2.81%	–
	$\epsilon = 3.5\%$	27.25	4.06×10^{-8}	1.99%	–
	$\epsilon = 3.0\%$	27.65	4.03×10^{-8}	1.76%	–
	$\epsilon = 2.5\%$	29.95	4.04×10^{-8}	1.53%	–
	$\epsilon = 2.0\%$	31.90	4.02×10^{-8}	1.00%	–

mean failure probability value with a very small COV, but at the cost of an average of 282.30 performance function calls. PBALC1, PBACL2, PBALC3, SBALQ and QBALC are able to reduce the average number of $\mathcal{G}$-function evaluations significantly, while still producing quite good results. For the case of $\epsilon = 4.0\%$, the proposed WBALQ method demonstrates comparable unbiasedness and variability, but requires fewer g-function evaluations on average compared to the aforementioned five methods. Overall, as ϵ decreases, the performance of the proposed method improves, albeit with an increase in the average number of performance function evaluations.

4.3. Example 3: An I beam

The third numerical example consists of a simply-supported I beam under a concentrated force [39], which is shown in Fig. 5. The performance function is expressed as follows:

$$g(\boldsymbol{X}) = S - \sigma_{\max}, \tag{32}$$

in which

$$\sigma_{\max} = \frac{Pa(L-a)d}{2LI}, \tag{33}$$

with

$$I = \frac{b_f d^3 - (b_f - t_w)(d - 2t_f)^3}{12}. \tag{34}$$

Eight basic random variables $\boldsymbol{X} = [P, L, a, S, d, b_f, t_w, t_f]$ are involved in the performance function (Eq. (32)), as described in Table 5.

Table 5
Basic random variables for Example 3.

Variable	Distribution	Mean	COV
P	Gumbel	1500	0.15
L	Normal	120	0.05
a	Normal	72	0.10
S	Normal	200,000	0.15
d	Normal	2.3	0.05
b_f	Normal	2.3	0.05
t_w	Normal	0.16	0.05
t_f	Normal	0.26	0.05

Table 6
Reliability analysis results of Example 3 by several methods.

Method		N_{call}	$\hat{P}_f$	$\delta_{\hat{P}_f}$
MCS	–	10^{11}	1.16×10^{-7}	0.93%
AK-MCMC	–	390.05	1.16×10^{-7}	2.23%
PBALC1	$\epsilon_1 = 5.0\%$	46.35	1.16×10^{-7}	3.46%
PBALC2	$\epsilon_2 = 5.0\%$	50.40	1.15×10^{-7}	2.72%
PBALC3	$\epsilon_3 = 10.0\%$	49.15	1.15×10^{-7}	3.48%
SBALQ	$\epsilon = 4.0\%$	47.45	1.14×10^{-7}	3.91%
QBALC	$\epsilon = 5.0\%$	45.80	1.14×10^{-7}	3.10%
Proposed WBALQ	$\epsilon = 5.0\%$	33.55	1.14×10^{-7}	6.34%
	$\epsilon = 4.5\%$	34.65	1.14×10^{-7}	5.82%
	$\epsilon = 4.0\%$	37.05	1.13×10^{-7}	3.76%
	$\epsilon = 3.5\%$	40.40	1.13×10^{-7}	3.30%
	$\epsilon = 3.0\%$	42.40	1.14×10^{-7}	3.44%
	$\epsilon = 2.5\%$	46.30	1.14×10^{-7}	3.27%
	$\epsilon = 2.0\%$	50.70	1.14×10^{-7}	2.33%

The main results of several methods, i.e., MCS, AK-MCMC, PBALC1, PBACL2, PBALC3, SBALQ, QBALC and WBALQ, are summarized in Table 6. The reference solution for the failure probability provided by MCS with 10^{11} samples is 1.16×10^{-7} with a COV of 0.93%. All the six methods, i.e., AK-MCMC, PBALC1, PBACL2, PBALC3, SBALQ and QBALC, can give satisfactory results for the failure probability. Among these, the last five methods require on average significantly fewer g-function evaluations than AK-MCMC. In all cases studied except for $\epsilon = 5.0\%$ and $\epsilon = 4.5\%$, the proposed WBALQ method provides an unbiased mean value of the failure probability with a COV of less than 5%. Specifically, for $\epsilon = 4.0\%$, the proposed WBALQ method outperforms PBALC1, PBACL2, PBALC3, SBALQ, and QBALC in terms of the average number of performance function evaluations.

4.4. Example 4: A space truss structure

The fourth numerical example involves a 56-bar space truss structure [40], as depicted in Fig. 6. The finite element model of this structure is established using OpenSees with 56 elements and 25 nodes. Assume that the Young's modulus and the cross-sectional area are the same for each element, denoted E and A respectively. Nine concentrated loads, $P_1, P_2, \ldots, P_9$, are applied to nodes $1 \sim 9$ along the negative of the z axis. Once the vertical displacement of the top node exceeds a

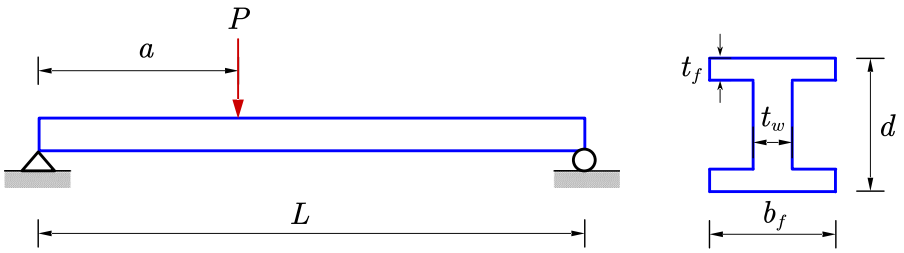

Fig. 5. A simply-supported I beam subjected to a concentrated force.

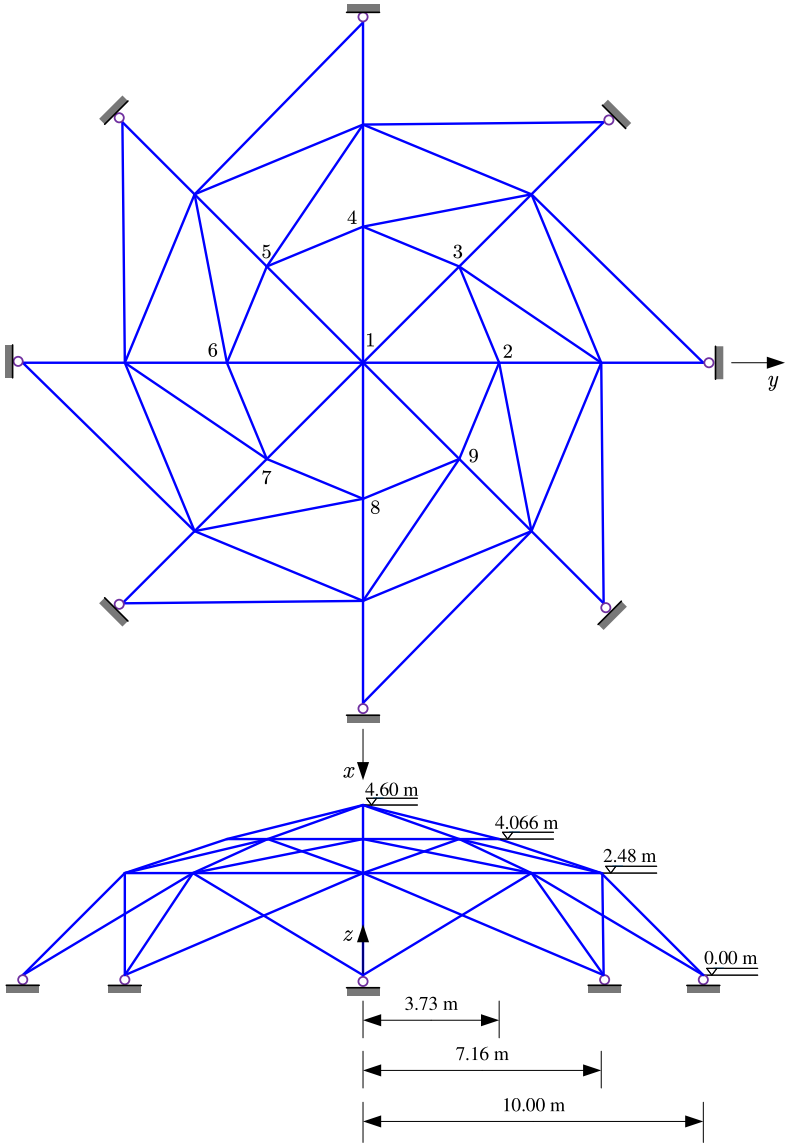

Fig. 6. Schematic diagram of a 56-bar space truss structure.

certain threshold, a failure is considered to have occurred, resulting in the following performance function:

$$g(\boldsymbol{X}) = \Delta - V_1(P_1 \sim P_9, E, A), \tag{35}$$

where Δ denotes the threshold, which is specified as 50 mm; V_1 is the vertical displacement of node 1; $P_1 \sim P_9$, E and A are eleven basic random variables, as listed in Table 7.

In this example, the IS method available in UQLab [41] is employed to provide a reference solution. The failure probability value obtained is 4.94×10^{-8} with a COV of 1.00%, using 66,107 g-function calls. The results of IS and several other methods are reported in Table 8. It can be seen that AK-MCMC can produce very good results, but at the cost of an average of 465.00 g-function calls, which is far more than other methods (except IS). Besides, the proposed method (ϵ = 4.0%)

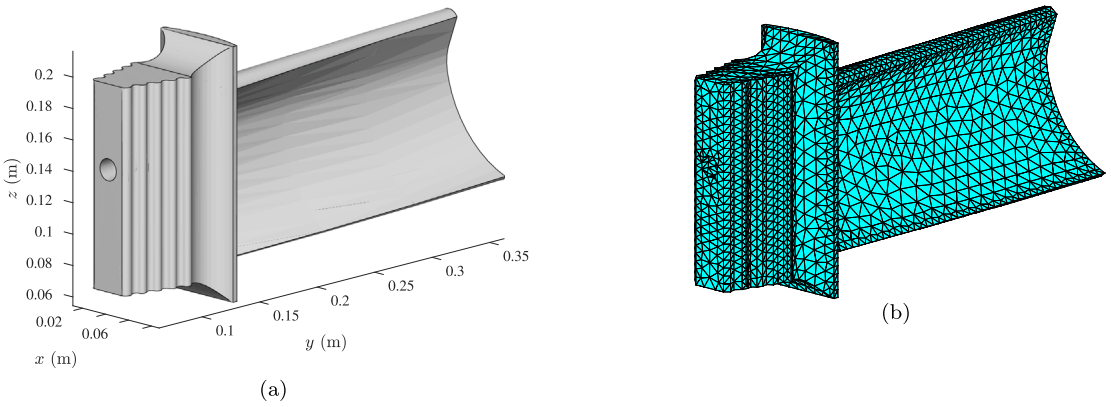

Fig. 7. A jet engine turbine blade: (a) Geometry; (b) Mesh.

Table 7
Basic random variables for Example 4.

Variable	Distribution	Mean	COV
P_1	Lognormal	150 kN	0.20
$P_2 \sim P_9$	Lognormal	100 kN	0.20
E	Normal	2.06 GPa	0.10
A	Normal	2000 mm^2	0.05

Table 8
Reliability analysis results of Example 4 by several methods.

Method		N_{call}	$\hat{P}_f$	$\delta_{\hat{P}_f}$	Reference
IS	–	66,107	4.94×10^{-8}	1.00%	[35]
AK-MCMC	–	465.00	4.97×10^{-8}	2.92%	[35]
PBALC1	$\epsilon_1 = 5.0\%$	27.20	4.86×10^{-8}	5.70%	[32]
PBALC2	$\epsilon_2 = 5.0\%$	26.90	4.85×10^{-8}	4.61%	[32]
PBALC3	$\epsilon_3 = 10.0\%$	26.30	4.87×10^{-8}	6.64%	[32]
SBALQ	$\epsilon = 4.0\%$	31.40	4.77×10^{-8}	5.32%	–
QBALC	$\epsilon = 5.0\%$	29.20	4.69×10^{-8}	6.42%	–
	$\epsilon = 5.0\%$	24.90	4.76×10^{-8}	8.98%	–
	$\epsilon = 4.5\%$	25.75	4.80×10^{-8}	8.91%	–
	$\epsilon = 4.0\%$	26.30	4.87×10^{-8}	5.57%	–
Proposed WBALQ	$\epsilon = 3.5\%$	27.50	4.90×10^{-8}	4.87%	–
	$\epsilon = 3.0\%$	29.05	4.97×10^{-8}	4.48%	–
	$\epsilon = 2.5\%$	31.05	4.92×10^{-8}	2.85%	–
	$\epsilon = 2.0\%$	32.40	4.97×10^{-8}	1.68%	–

Table 9
Basic random variables for Example 5.

Variable	Distribution	Mean	COV
E	Normal	220 GPa	0.10
ν	Normal	0.30	0.05
κ	Uniform	1.25×10^{-7} 1/K	0.05
p_1	Gumbel	500 kPa	0.15
p_2	Gumbel	450 kPa	0.15

Table 10
Reliability analysis results of Example 5 by several methods.

Method		N_{call}	$\hat{P}_f$	$\delta_{\hat{P}_f}$	Time (s)
AK-MCMC	–	231.95	1.17×10^{-8}	11.60%	231.95
PBALC1	$\epsilon_1 = 5.0\%$	27.15	1.25×10^{-8}	5.03%	234.67
PBALC2	$\epsilon_2 = 5.0\%$	29.10	1.25×10^{-8}	2.64%	265.18
PBALC3	$\epsilon_3 = 10.0\%$	27.65	1.24×10^{-8}	2.28%	246.89
SBALQ	$\epsilon = 4.0\%$	27.80	1.22×10^{-8}	6.47%	195.27
QBALC	$\epsilon = 5.0\%$	26.70	1.22×10^{-8}	7.06%	329.49
	$\epsilon = 5.0\%$	22.00	1.22×10^{-8}	6.13%	103.55
	$\epsilon = 4.5\%$	22.80	1.24×10^{-8}	5.74%	111.58
	$\epsilon = 4.0\%$	23.40	1.23×10^{-8}	4.46%	114.06
Proposed WBALQ	$\epsilon = 3.5\%$	24.05	1.25×10^{-8}	2.10%	126.15
	$\epsilon = 3.0\%$	25.15	1.24×10^{-8}	2.52%	139.04
	$\epsilon = 2.5\%$	28.55	1.25×10^{-8}	1.31%	172.81
	$\epsilon = 2.0\%$	28.25	1.26×10^{-8}	1.76%	176.00

performs similarly to PBALC1, PBALC2 and PBALC3, and slightly better than SBALQ and QBALC in terms of the average number of model evaluations.

4.5. Example 5: A jet engine turbine blade

The final example is a turbine blade in a jet engine (shown in Fig. 7(a)), which extracts energy from high-temperature, high-pressure gas and converts it into rotational motion to generate thrust. This model is available in the Partial Differential Equation Toolbox of Matlab R2023a. The turbine blade is made of a nickel-based alloy (NIMONIC 90), with material properties including Young's modulus E, Poisson's ratio υ, coefficient of thermal expansion κ. For the boundary condition, the surface of the root in contact with the other metal is fixed. The pressure and suction sides of the blade are subject to pressure loads p_1 and p_2, respectively. As depicted in Fig. 7(b), the finite element model is generated using a tetrahedral mesh with the maximum element size of 0.01 m. A common cause of turbine blade failure is stress exceeding the stress limit of the material, so the following performance function is considered:

$$g(\boldsymbol{X}) = \sigma_{\text{th}} - \sigma_{\max}\left(E, \upsilon, \kappa, p_1, p_2\right), \tag{36}$$

where $\sigma_{\max}$ is the maximum von Mises stress of the blade; σ_{th} is the associated threshold, which is specified as 0.8 GPa; E, υ, κ, p_1 and p_2 are treated as random variables, as detailed in Table 9.

The reliability analysis results obtained by several different methods are summarized in Table 10. The simulations were performed on a computer with an AMD Ryzen Threadripper PRO 5975WX processor, 64 GB of RAM. The reference failure probability is taken as 1.24×10^{-8} with a COV of 2.28%, produced by PBALC3 with an average of 27.65 performance function evaluations. AK-MCMC requires, on average, 231.95 performance function calls, while producing a slightly biased mean for the failure probability, with a large COV up to 11.60%. The average computation time is 231.95 s. The other methods (i.e., PBALC1, PBALC2, PBALC3, SBALQ, QBALC and WBALQ) perform much better than AK-MCMC. Taking $\epsilon = 3.5\%$ as an example, the proposed WBALQ method gives fairly good results, while requiring fewer g-function calls and less computation time on average among them.

Remark. In the five numerical examples above, we have studied the effect of the stopping criterion threshold ϵ on the performance of our method. It is shown empirically that: (1) a large ϵ (e.g., 5.0%) can lead

to a high bias and a large COV for the probability of failure; (2) a small ϵ (e.g., 2.0%) can lead to a low (or almost no) bias and a rather small COV for the probability of failure. As a compromise, $\epsilon = 4.0\%$ can be adopted to produce a COV for the failure probability around 5%, while with an acceptable bias.

5. Concluding remarks

In this work, another novel Bayesian active learning method, termed 'weakly Bayesian active learning quadrature' (WBALQ), is presented for structural reliability analysis, particularly for evaluating extremely small failure probabilities. The proposed method is grounded in the well-established Bayesian failure probability inference framework. The main contributions lie in the development of two key components (i.e., stopping criterion and learning function) for Bayesian active learning of the failure probability without relying on the posterior variance of the failure probability (which is computationally prohibitive). This is achieved by examining the upper bound of the first absolute central moment of the posterior failure probability instead. Utilizing this upper bound and the posterior mean of the failure probability, we devise a new stopping criterion involving two analytically intractable integrals. These integrals are then solved using a recently developed numerical integration scheme. A new learning function, called 'Weighted Epistemic Uncertainty Contribution' (WEUC), is also developed in light of the upper bound. By studying five numerical examples, it is empirically shown that the proposed WBALQ method: (1) can estimate extremely small failure probabilities (on the order of 10^{-9} - 10^{-7}); (2) performs much better, or at least similarly, to several existing methods. In addition, $\epsilon = 4.0\%$ is recommended for the stopping criterion of the proposed method.

Admittedly, the proposed method has difficulties in dealing with high dimensional and/or highly non-linear problems. A possible research direction to improve its performance in high dimensions is to incorporate dimension reduction techniques. While for dealing with highly non-linear problems, a possible way is to use other kernels instead of the Gaussian one, or even other Bayesian models instead of the GP.

CRediT authorship contribution statement

Chao Dang: Writing – review & editing, Writing – original draft, Visualization, Validation, Methodology, Investigation, Conceptualization. **Tong Zhou:** Writing – review & editing, Conceptualization. **Marcos A. Valdebenito:** Writing – review & editing, Supervision, Conceptualization. **Matthias G.R. Faes:** Writing – review & editing, Supervision, Project administration, Funding acquisition.

Declaration of competing interest

The authors declare that they have no known competing financial interests or personal relationships that could have appeared to influence the work reported in this paper.

Data availability

No data was used for the research described in the article.

Acknowledgments

Chao Dang is grateful for the financial support of the German Research Foundation (DFG) (Grant number 530326817).

References

[1] Freudenthal AM. The safety of structures. Trans Am Soc Civ Eng 1947;112(1):125–59. http://dx.doi.org/10.1061/TACEAT.0006015.
[2] Freudenthal AM. Safety and the probability of structural failure. Trans Am Soc Civ Eng 1956;121(1):1337–75. http://dx.doi.org/10.1061/TACEAT.0007306.
[3] Melchers R. Importance sampling in structural systems. Struct Saf 1989;6(1):3–10. http://dx.doi.org/10.1016/0167-4730(89)90003-9.
[4] Au S-K, Beck JL. A new adaptive importance sampling scheme for reliability calculations. Struct Saf 1999;21(2):135–58. http://dx.doi.org/10.1016/S0167-4730(99)00014-4.
[5] Geyer S, Papaioannou I, Straub D. Cross entropy-based importance sampling using Gaussian densities revisited. Struct Saf 2019;76:15–27. http://dx.doi.org/10.1016/j.strusafe.2018.07.001.
[6] Dasgupta A, Johnson EA. REIN: Reliability estimation via importance sampling with normalizing flows. Reliab Eng Syst Saf 2024;242:109729. http://dx.doi.org/10.1016/j.ress.2023.109729.
[7] Au S-K, Beck JL. Estimation of small failure probabilities in high dimensions by subset simulation. Probab Eng Mech 2001;16(4):263–77. http://dx.doi.org/10.1016/S0266-8920(01)00019-4.
[8] Papaioannou I, Betz W, Zwirglmaier K, Straub D. MCMC algorithms for subset simulation. Probab Eng Mech 2015;41:89–103. http://dx.doi.org/10.1016/j.probengmech.2015.06.006.
[9] Wang Z, Broccardo M, Song J. Hamiltonian Monte Carlo methods for subset simulation in reliability analysis. Struct Saf 2019;76:51–67. http://dx.doi.org/10.1016/j.strusafe.2018.05.005.
[10] Nie J, Ellingwood BR. Directional methods for structural reliability analysis. Struct Saf 2000;22(3):233–49. http://dx.doi.org/10.1016/S0167-4730(00)00014-X.
[11] Nie J, Ellingwood BR. A new directional simulation method for system reliability. Part I: application of deterministic point sets. Probab Eng Mech 2004;19(4):425–36. http://dx.doi.org/10.1016/j.probengmech.2004.03.004.
[12] Koutsourelakis P-S, Pradlwarter HJ, Schueller GI. Reliability of structures in high dimensions, part I: algorithms and applications. Probab Eng Mech 2004;19(4):409–17. http://dx.doi.org/10.1016/j.probengmech.2004.05.001.
[13] de Angelis M, Patelli E, Beer M. Advanced line sampling for efficient robust reliability analysis. Struct Saf 2015;52:170–82. http://dx.doi.org/10.1016/j.strusafe.2014.10.002.
[14] Papaioannou I, Straub D. Combination line sampling for structural reliability analysis. Struct Saf 2021;88:102025. http://dx.doi.org/10.1016/j.strusafe.2020.102025.
[15] Hasofer AM, Lind NC. Exact and invariant second-moment code format. J Eng Mech Div 1974;100(1):111–21. http://dx.doi.org/10.1061/JMCEA3.0001848.
[16] Breitung KW. Asymptotic approximations for probability integrals. Springer; 2006.
[17] Zhao Y-G, Lu Z-H. Structural reliability: approaches from perspectives of statistical moments. John Wiley & Sons; 2021.
[18] Zhang X, Pandey MD. Structural reliability analysis based on the concepts of entropy, fractional moment and dimensional reduction method. Struct Saf 2013;43:28–40. http://dx.doi.org/10.1016/j.strusafe.2013.03.001.
[19] Xu J, Yu Q. Harmonic transform-based non-parametric density estimation method for forward uncertainty propagation and reliability analysis. Struct Saf 2023;103:102331. http://dx.doi.org/10.1016/j.strusafe.2023.102331.
[20] Bucher CG, Bourgund U. A fast and efficient response surface approach for structural reliability problems. Struct Saf 1990;7(1):57–66. http://dx.doi.org/10.1016/0167-4730(90)90012-E.
[21] Blatman G, Sudret B. An adaptive algorithm to build up sparse polynomial chaos expansions for stochastic finite element analysis. Probab Eng Mech 2010;25(2):183–97. http://dx.doi.org/10.1016/j.probengmech.2009.10.003.
[22] Bourinet J-M. Rare-event probability estimation with adaptive support vector regression surrogates. Reliab Eng Syst Saf 2016;150:210–21. http://dx.doi.org/10.1016/j.ress.2016.01.023.
[23] Kaymaz I. Application of kriging method to structural reliability problems. Struct Saf 2005;27(2):133–51. http://dx.doi.org/10.1016/j.strusafe.2004.09.001.
[24] Song C, Kawai R. Monte Carlo and variance reduction methods for structural reliability analysis: A comprehensive review. Probab Eng Mech 2023;103479. http://dx.doi.org/10.1016/j.probengmech.2023.103479.
[25] Bichon BJ, Eldred MS, Swiler LP, Mahadevan S, McFarland JM. Efficient global reliability analysis for nonlinear implicit performance functions. AIAA J 2008;46(10):2459–68. http://dx.doi.org/10.2514/1.34321.
[26] Echard B, Gayton N, Lemaire M. AK-MCS: an active learning reliability method combining kriging and Monte Carlo simulation. Struct Saf 2011;33(2):145–54. http://dx.doi.org/10.1016/j.strusafe.2011.01.002.
[27] Teixeira R, Nogal M, O'Connor A. Adaptive approaches in metamodel-based reliability analysis: A review. Struct Saf 2021;89:102019. http://dx.doi.org/10.1016/j.strusafe.2020.102019.
[28] Moustapha M, Marelli S, Sudret B. Active learning for structural reliability: Survey, general framework and benchmark. Struct Saf 2022;96:102174. http://dx.doi.org/10.1016/j.strusafe.2021.102174.

[29] Dang C, Wei P, Song J, Beer M. Estimation of failure probability function under imprecise probabilities by active learning–augmented probabilistic integration. ASCE-ASME J Risk Uncertain Eng Syst A 2021;7(4):04021054. http://dx.doi.org/10.1061/AJRUA6.0001179.

[30] Dang C, Wei P, Faes MG, Valdebenito MA, Beer M. Parallel adaptive Bayesian quadrature for rare event estimation. Reliab Eng Syst Saf 2022;225:108621. http://dx.doi.org/10.1016/j.ress.2022.108621.

[31] Dang C, Valdebenito MA, Faes MG, Wei P, Beer M. Structural reliability analysis: A Bayesian perspective. Struct Saf 2022;99:102259. http://dx.doi.org/10.1016/j.strusafe.2022.102259.

[32] Dang C, Faes MG, Valdebenito MA, Wei P, Beer M. Partially Bayesian active learning cubature for structural reliability analysis with extremely small failure probabilities. Comput Methods Appl Mech Engrg 2024;422:116828. http://dx.doi.org/10.1016/j.cma.2024.116828.

[33] Dang C, Beer M. Semi-Bayesian active learning quadrature for estimating extremely low failure probabilities. Reliab Eng Syst Saf 2024;110052. http://dx.doi.org/10.1016/j.ress.2024.110052.

[34] Hu Z, Dang C, Wang L, Beer M. Parallel Bayesian probabilistic integration for structural reliability analysis with small failure probabilities. Struct Saf 2024;106:102409. http://dx.doi.org/10.1016/j.strusafe.2023.102409.

[35] Dang C, Cicirello A, Valdebenito MA, Faes MG, Wei P, Beer M. Structural reliability analysis with extremely small failure probabilities: A quasi-Bayesian active learning method. Probab Eng Mech 2024;76:103613. http://dx.doi.org/10.1016/j.probengmech.2024.103613.

[36] Zhou T, Guo T, Dang C, Beer M. Bayesian reinforcement learning reliability analysis. Comput Methods Appl Mech Engrg 2024;424:116902. http://dx.doi.org/10.1016/j.cma.2024.116902.

[37] Su M, Xue G, Wang D, Zhang Y, Zhu Y. A novel active learning reliability method combining adaptive kriging and spherical decomposition-MCS (AK-SDMCS) for small failure probabilities. Struct Multidiscip Optim 2020;62:3165–87. http://dx.doi.org/10.1007/s00158-020-02661-w.

[38] Wei P, Tang C, Yang Y. Structural reliability and reliability sensitivity analysis of extremely rare failure events by combining sampling and surrogate model methods. Proc Inst Mech Eng O 2019;233(6):943–57. http://dx.doi.org/10.1177/1748006X19844666.

[39] Huang B, Du X. Uncertainty analysis by dimension reduction integration and saddlepoint approximations. J Mech Des 2006;128(1):26–33. http://dx.doi.org/10.1115/1.2118667.

[40] Dang C, Wei P, Faes MG, Beer M. Bayesian probabilistic propagation of hybrid uncertainties: Estimation of response expectation function, its variable importance and bounds. Comput Struct 2022;270:106860. http://dx.doi.org/10.1016/j.compstruc.2022.106860.

[41] Marelli S, Schöbi R, Sudret B. UQLab user manual – Structural reliability (Rare event estimation). Tech. rep., Chair of Risk, Safety and Uncertainty Quantification, ETH Zurich, Switzerland; 2022, Report UQLab-V2.0-107.